NASA TECHNICAL REPORT

NASA TR R-227

NASA TR R-227

c 1

[illegible COPY]
AFWL (WLIL-2)
KIRTLAND AFB, N MEX

TECH LIBRARY KAFB, NM
0068507

A THEORETICAL AND EXPERIMENTAL STUDY OF THE NONLINEAR FLEXURAL VIBRATIONS OF THIN CIRCULAR RINGS

by David A. Evensen

Langley Research Center
Langley Station, Hampton, Va.

NATIONAL AERONAUTICS AND SPACE ADMINISTRATION • WASHINGTON, D. C. • DECEMBER 1965

TECH LIBRARY KAFB, NM
0068507
NASA TR R-227

A THEORETICAL AND EXPERIMENTAL STUDY OF THE NONLINEAR FLEXURAL VIBRATIONS OF THIN CIRCULAR RINGS

By David A. Evensen

Langley Research Center
Langley Station, Hampton, Va.

NATIONAL AERONAUTICS AND SPACE ADMINISTRATION

For sale by the Clearinghouse for Federal Scientific and Technical Information
Springfield, Virginia 22151 – Price $3.00

CONTENTS

A THEORETICAL AND EXPERIMENTAL STUDY OF THE NONLINEAR FLEXURAL VIBRATIONS OF THIN CIRCULAR RINGS

By David A. Evensen
Langley Research Center

SUMMARY

The nonlinear flexural vibrations of thin circular rings are analyzed by assuming two vibration modes and then applying Galerkin's procedure on the equations of motion. This procedure results in coupled nonlinear ordinary differential equations with time as the independent variable. The applied loading is taken to be harmonic in time, and approximate solutions to the equations are obtained by the method of averaging. One such solution involves the vibration of a single bending mode; a subsequent stability analysis shows that this single-mode response is valid only for certain combinations of amplitude and frequency. For example, when the driven mode exceeds a critical amplitude, nonlinear coupling causes its companion mode to respond and participate in the motion. Approximate solutions are obtained for this coupled-mode case, and their stability is examined. The steady-state response curves contain an unusual "gap," where both the one- and two-mode solutions are unstable. These results were confirmed on an analog computer, and nonsteady vibrations were observed in the gap region.

An experimental study of the problem was also conducted. Theory and experiment both indicate a nonlinearity of the softening type and the appearance of the companion mode. Measurements of the steady-state response are in good agreement with the calculated values, and the experimentally determined mode shapes agree with the form of the assumed deflection.

The analytical and experimental results exhibit several features that are characteristic of nonlinear vibrations of axisymmetric systems in general and of circular cylindrical shells in particular.

INTRODUCTION

Current design of launch vehicles relies heavily on the use of thin-walled cylindrical shells as the primary structure. During powered flight, these cylindrical structures are often caused to vibrate to large amplitudes, in response to their environment. This problem has given rise to a number of theoretical studies of the nonlinear vibrations of thin cylindrical shells

(refs. 1 to 3). However, recent experimental results (ref. 4) suggest that such vibrations are still not fully understood. These studies prompted the investigation of a simpler but related problem, namely, the nonlinear flexural vibrations of a thin circular ring.

Flexural vibrations of circular rings were originally analyzed in 1871 by Hoppe (ref. 5), who presented the linear vibration frequencies and mode shapes. Shortly thereafter, Rayleigh (ref. 6) obtained similar results by using the approximation that the midsurface of the ring was inextensional. Since that time, the effects of midsurface extension, shear deformation, and rotary inertia have been investigated (refs. 7 to 9).

The first study of the elastic, nonlinear flexural vibrations of rings appears to be the 1959 work of Federhofer (ref. 10), who analyzed the free-vibration problem. The same problem was examined by Shkenyev (ref. 11), who was primarily concerned with the dynamic stability of rings, as were Goodier and McIvor (ref. 12). No experiments on the nonlinear vibration of rings have been reported in the literature, although linear vibrations have been studied experimentally (refs. 13 and 14).

The purpose of the present work is to study the forced, nonlinear flexural vibrations of thin circular rings. Only vibrations in the plane of the ring are considered, and the stress-strain law (Hooke's Law) is assumed to be linear. The nonlinearities examined here are geometric in nature and arise from the nonlinear terms of the strain-displacement relations. The ring is assumed to be of uniform rectangular cross section and to be relatively thin. With these restrictions, a detailed theoretical and experimental study of the problem was conducted.

Agreement between theory and experiment was generally very good. The calculated response curves compare favorably with the experimental results, and measurements of the actual vibration form confirm the choice of the mode shapes used in the analysis. Both theory and experiment exhibit coupled vibrations that involve a driven mode and its companion mode. The results demonstrate several features that are characteristic of nonlinear vibrations of axisymmetric systems in general and of circular cylindrical shells in particular.

This research was conducted while the author was a graduate student at the California Institute of Technology; the present report is a condensation of reference 15.

SYMBOLS

The units used for the physical quantities defined in this paper are given both in U.S. Customary Units and in the International System of Units (SI) (ref. 16). Appendix A presents factors relating these two systems.

$A_o(t)$ amplitude and time-varying part of uniform contraction, in. (cm) (see eqs. (8) and (9))

$A_n(t), B_n(t)$ generalized coordinates associated with $\cos \frac{ny}{R}$ and $\sin \frac{ny}{R}$ modes, in. (cm) (see eqs. (8) and (10))

$A(\tau), B(\tau)$ slowly varying amplitudes, nondimensional

$A_E(t), B_E(t), C_E(t)$ experimental amplitudes

$\bar{A}_o, \bar{B}_o$ and $\bar{\Phi}_o, \bar{\Psi}_o$ steady-state values of amplitudes and phases, respectively (see eqs. (F2))

b ring length, in. (cm)

D bending stiffness, $\frac{Eh^3}{12(1 - \nu^2)}$, in-lb (m-N)

d displacement, in. (cm) (see fig. 14)

E Young's modulus, lb/in^2 (N/m^2)

e base of Napierian logarithm

F load per unit length applied to ring in experiment, lb/in. (N/m)

F_n magnitude of assumed loading, lb/in. (N/m) (see eq. (13))

G_n dimensionless force

h ring thickness, in. (cm)

i,j integers

K,Q Mathieu equation coefficients

k spring constant of drive wire, lb/in. (N/m)

M_x, M_{xy}, M_y resultant moments per unit length, in-lb/in. (m-N/m)

N_x, N_{xy}, N_y resultant forces per unit length, lb/in. (N/m)

n number of circumferential waves (n = 2, 3, 4, . . .)

P magnitude of load experimentally applied to ring, lb (N)

q(x,y,t) radial load applied to cylinder

$q(y,t)$ radial load applied to ring

R mean radius of ring, in. (cm)

r fraction of half wavelength

t time, sec

U stability variable used in equations (D7)

u,v,w displacement of a point on middle surface in axial, tangential, and radial direction, respectively

x,y,z coordinate in axial, circumferential, and radial direction, respectively

Y,Z Mathieu equation variables

β_c,β_s percent critical damping in $\cos\frac{ny}{R}$ and $\sin\frac{ny}{R}$ mode, respectively

$\bar{\Delta} = \bar{\psi} - \bar{\Phi}$

δ_o amplitude of shaker displacement, in. (cm)

ϵ dimensionless nonlinearity parameter, $\left(\frac{n^2h}{R}\right)^2$

ϵ_c corrected nonlinearity parameter (see eq. (29))

$\epsilon_i = \epsilon\left(\frac{n}{n^2+1}\right)\left(1+\frac{1}{8n^2}\right)$

$\epsilon_{xx},\epsilon_{yy}$ direct strains

$\epsilon_{xy},\epsilon_{xz},\epsilon_{yz}$ shear strains

$\zeta_c(\tau),\zeta_s(\tau)$ nondimensional generalized coordinate associated with $\cos\frac{ny}{R}$ and $\sin\frac{ny}{R}$ mode, respectively

λ,λ_i nondimensional stability variables

$\mu = \frac{\epsilon\bar{A}^2}{2}$

ν Poisson's ratio

$\xi_c(\tau), \xi_s(\tau)$ perturbation in response of $\cos \frac{ny}{R}$ and $\sin \frac{ny}{R}$ mode, respectively (see eqs. (D1) and (D2))

ρ mass density, lb-sec^2/in^4 (kg/m^3)

$\sigma_{xx}, \sigma_{yy}, \sigma_{zz}$ normal stresses, lb/in^2 (N/m^2)

σ_{xy} shear stress, lb/in^2 (N/m^2)

τ nondimensional time, $\omega_M t$

Φ_A, Φ_B experimental phases

$\Phi(\tau), \psi(\tau)$ slowly varying phases, nondimensional

$\chi = \Omega\tau + \Phi$

Ω nondimensional frequency, ω/ω_M

ω vibration frequency, radians/sec

ω_c linear frequency of $\cos \frac{ny}{R}$; driven mode (see fig. 15)

ω_L nth linear vibration frequency, $\left[\frac{E}{\rho R^2} \frac{n^2}{(n^2 + 1)} \frac{(n^2 - 1)^2}{12(1 - \nu^2)}\left(\frac{h}{R}\right)^2\right]^{1/2}$, radians/sec

ω_M approximate vibration frequency, $\left[\frac{E}{\rho R^2} \frac{(n^2 - 1)^2}{12(1 - \nu^2)}\left(\frac{h}{R}\right)^2\right]^{1/2}$, radians/sec

ω_s linear frequency of $\sin \frac{ny}{R}$; companion mode (see fig. 15)

∇^2 Laplacian operator, $\frac{\partial^2}{\partial x^2} + \frac{\partial^2}{\partial y^2}$

∇^4 biharmonic operator, $\nabla^2\nabla^2$

$O(\epsilon^2)$ order ϵ^2

Subscripts:

cr	critical
max	maximum

A dot over a quantity indicates differentiation with respect to time; a bar over a quantity indicates an average value.

THEORY

In this report, the nonlinear vibrations of a thin ring are analyzed by approximate techniques. The governing equations of motion are presented first, along with the associated boundary conditions. These equations are then reduced to ordinary differential equations by applying Galerkin's procedure. Two coupled nonlinear equations result, and approximate solutions to them are obtained by the method of averaging. The stability of these solutions is examined, and improvements in the analysis are discussed.

Equations of Motion

The nonlinear equations of motion of a thin ring can be written in the form (see appendix B)

$$\frac{\partial N_y}{\partial y} = \rho h \frac{\partial^2 v}{\partial t^2} \tag{1a}$$

$$D\left(\frac{\partial^2}{\partial y^2} + \frac{1}{R^2}\right)\left(\frac{\partial^2 w}{\partial y^2} + \frac{w}{R^2}\right) + \frac{N_y}{R} - \frac{\partial}{\partial y}\left(N_y \frac{\partial w}{\partial y}\right) + \rho h \frac{\partial^2 w}{\partial t^2} = q(y,t) \tag{1b}$$

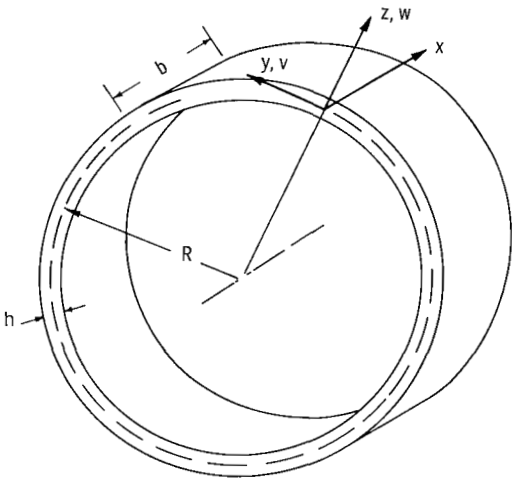

Figure 1.- Ring geometry and coordinate system.

where the circumferential force is given by

$$N_y = Eh\left[\frac{\partial v}{\partial y} + \frac{w}{R} + \frac{1}{2}\left(\frac{\partial w}{\partial y}\right)^2\right] \tag{2}$$

and the radial displacement w, the tangential displacement v, and the applied load q are taken to be functions of only the circumferential coordinate y and the time t. (See fig. 1.) These results are obtained by a specialization of the analogous equations for thin cylindrical shells.

Boundary conditions.- Since the ring is circular, the displacements must satisfy the following continuity requirements:

$$\left.\begin{aligned} w(y,t) &= w(y + 2\pi R,t) \\ \frac{\partial^i w}{\partial y^i}(y,t) &= \frac{\partial^i w}{\partial y^i}(y + 2\pi R,t) \qquad (i = 1, 2) \end{aligned}\right\} \tag{3a}$$

$$\left.\begin{aligned} v(y,t) &= v(y + 2\pi R,t) \\ \frac{\partial v}{\partial y}(y,t) &= \frac{\partial v}{\partial y}(y + 2\pi R,t) \end{aligned}\right\} \tag{3b}$$

in addition to the equations of motion. From a physical standpoint, these boundary conditions insure that the displacements, slope, and other related variables are continuous in the circumferential direction.

Simplified equations of motion.- Previous work (ref. 15) has shown that for flexural vibrations, equations (1) can be simplified considerably without losing the essential features of the problem. This simplification is accomplished by

(1) assuming that the midsurface circumferential strain is zero

(2) neglecting the effect of tangential inertia

The first of these conditions requires

$$\epsilon_{yy}\Big|_{z=0} = \frac{\partial v}{\partial y} + \frac{w}{R} + \frac{1}{2}\left(\frac{\partial w}{\partial y}\right)^2 = 0 \tag{4}$$

where the nonlinear strain-displacement relations (appendix B) have been used. Similarly, neglecting tangential inertia in equation (1a) results in

$$\frac{\partial N_y}{\partial y} = 0 \tag{5}$$

Combining equations (2), (4), and (5) gives $N_y = 0$. Using this result in equation (1b) yields the simplified equation of motion for w:

$$D\left(\frac{\partial^2}{\partial y^2} + \frac{1}{R^2}\right)\left(\frac{\partial^2 w}{\partial y^2} + \frac{w}{R^2}\right) + \rho h \frac{\partial^2 w}{\partial t^2} = q(y,t) \tag{6}$$

Note that the continuity conditions on w and v are not altered by the preceding discussion.

With these simplifications, the remaining problem is to solve equation (6) subject to the continuity and inextensionality constraints. Since the latter requirement (eq. (4)) is nonlinear and obviates exact solutions to equation (6), it is necessary to resort to approximate techniques.

Nonlinear Ordinary Differential Equations for Vibration of a Thin Circular Ring

Approximate solutions to equation (6) can be obtained by assuming the shape of the deflection in space. This approach is commonly used in nonlinear vibrations of structures (cf. refs. 17 to 19) and reduces the problem to one involving nonlinear ordinary differential equations in t.

Choice of deflection modes.- The most general radial deflection compatible with the continuity requirements is

$$w(y,t) = \sum_{n=0}^{\infty} \left[A_n(t)\cos \frac{ny}{R} + B_n(t)\sin \frac{ny}{R} \right] \tag{7}$$

where $A_n(t)$ and $B_n(t)$ are periodic in time. This case has been analyzed in detail in reference 15, but the majority of the results can be obtained by using the following two-mode approximation:

$$w(y,t) = A_n(t)\cos \frac{ny}{R} + B_n(t)\sin \frac{ny}{R} + A_o(t) \tag{8}$$

Here $\cos \frac{ny}{R}$ and $\sin \frac{ny}{R}$ are the linear vibration modes of the ring; and since only flexural motions are considered, equation (8) is restricted to cases where $n \geq 2$. The $n = 0$ mode is (by itself) an axisymmetric motion involving stretching of the midsurface, and the $n = 1$ modes correspond to displacement of the ring as a rigid body. The A_o term in equation (8) is related to A_n and B_n by the inextensionality constraint.

Determination of $A_o(t)$ in terms of $A_n(t)$ and $B_n(t)$.- Solving equation (4) for $\partial v/\partial y$ and substituting for w from equation (8) gives

$$\frac{\partial v}{\partial y} = -\frac{w}{R} - \frac{1}{2}\left(\frac{\partial w}{\partial y}\right)^2$$

$$= -\frac{A_o(t)}{R} - \frac{n^2}{4R^2}\left[A_n^2(t) + B_n^2(t)\right] + \text{Terms periodic in } y$$

To satisfy the constraint $v(y,t) = v(y + 2\pi R,t)$, the terms that depend solely on time must be equated to zero. This procedure yields

$$A_o(t) = -\frac{n^2}{4R}\left[A_n^2(t) + B_n^2(t)\right] \tag{9}$$

and equation (8) can then be rewritten as

$$w(y,t) = A_n(t)\cos\frac{ny}{R} + B_n(t)\sin\frac{ny}{R} - \frac{n^2}{4R}\left[A_n^2(t) + B_n^2(t)\right] \tag{10}$$

for the assumed radial displacement. This expression is compatible with the continuity and inextensionality constraints and can be used with Galerkin's procedure to satisfy approximately the simplified equation of motion for w.

Application of the Galerkin method.- To apply Galerkin's procedure, equation (10) is substituted for w in equation (6). The resulting expression is then multiplied by a weighting function associated with $A_n(t)$ and integrated with respect to y from 0 to $2\pi R$. This procedure yields an ordinary differential equation involving primarily $A_n(t)$. An equation for $B_n(t)$ is obtained in a similar fashion; both equations are coupled in the nonlinear terms. The weighting functions used are

$$\frac{\partial w}{\partial A_n} = \cos\frac{ny}{R} - \frac{n^2 A_n}{2R} \tag{11a}$$

and

$$\frac{\partial w}{\partial B_n} = \sin\frac{ny}{R} - \frac{n^2 B_n}{2R} \tag{11b}$$

respectively.

Carrying out the operations just indicated and then nondimensionalizing the results yields the following coupled equations:

$$\frac{d^2\zeta_c}{d\tau^2} + 2\beta_c\frac{d\zeta_c}{d\tau} + \zeta_c + \frac{\epsilon\zeta_c}{2}\left[\zeta_c\frac{d^2\zeta_c}{d\tau^2} + \left(\frac{d\zeta_c}{d\tau}\right)^2 + \zeta_s\frac{d^2\zeta_s}{d\tau^2} + \left(\frac{d\zeta_s}{d\tau}\right)^2\right] = G_n\cos\Omega\tau \tag{12a}$$

$$\frac{d^2\zeta_s}{d\tau^2} + 2\beta_s\frac{d\zeta_s}{d\tau} + \zeta_s + \frac{\epsilon\zeta_s}{2}\left[\zeta_s\frac{d^2\zeta_s}{d\tau^2} + \left(\frac{d\zeta_s}{d\tau}\right)^2 + \zeta_c\frac{d^2\zeta_c}{d\tau^2} + \left(\frac{d\zeta_c}{d\tau}\right)^2\right] = 0 \tag{12b}$$

where the dimensionless variables are

$$\zeta_c = \frac{A_n}{h} \qquad \zeta_s = \frac{B_n}{h}$$

$$\tau = \omega_M t \qquad \Omega = \frac{\omega}{\omega_M}$$

$$\epsilon = \left(\frac{n^2 h}{R}\right)^2 \qquad G_n = \frac{F_n}{\pi R \rho h^2 \omega_M^2}$$

and

(1) for simplicity, the loading has been taken to be

$$q(y,t) = \frac{F_n}{\pi R} \cos \frac{ny}{R} \cos \omega t \tag{13}$$

(2) two minor nonlinear terms have been discarded

(3) modal damping terms have been inserted to study the first-order effects of small viscous damping

Although these results were derived by a Galerkin procedure, they can also be obtained by the Rayleigh-Ritz method. In general, these two approximate techniques are not equivalent; they can be made to coincide, however, by the proper choice of weighting functions (ref. 20). It was for this reason that the weighting functions $\partial w/\partial A_n$ and $\partial w/\partial B_n$ were used to obtain equations (12).

Approximate Solutions to Nonlinear Equations

The previous section indicated the manner in which the equations of motion are reduced to ordinary nonlinear differential equations. These equations still cannot be solved exactly, but approximate solutions to them can be obtained by the "method of averaging." (For a discussion of this technique, see ref. 21, ch. V.)

Vibrations involving a single bending mode $\left(\cos \frac{ny}{R}\right)$ are considered first, and nonlinear single-mode response curves are presented. When the stability of the single-mode solution is examined, the vibrations are found to be stable for only certain combinations of amplitude and frequency; this result makes it necessary to examine vibrations where both $\cos \frac{ny}{R}$ and $\sin \frac{ny}{R}$ participate in the motion. The method of averaging is used to obtain approximate solutions for this two-mode case and also to examine their stability.

Response of a single bending mode.- Inspection of equations (12) reveals that possible solutions are $\zeta_s(\tau) = 0$ and $\zeta_c(\tau) \neq 0$, where the latter satisfies

$$\frac{d^2\zeta_c}{d\tau^2} + 2\beta_c \frac{d\zeta_c}{d\tau} + \zeta_c + \frac{\epsilon \zeta_c}{2}\left[\zeta_c \frac{d^2\zeta_c}{d\tau^2} + \left(\frac{d\zeta_c}{d\tau}\right)^2\right] = G_n \cos \Omega\tau \tag{14}$$

To obtain approximate solutions to equation (14) by the method of averaging, let

$$\zeta_c(\tau) = A(\tau)\cos\left[\Omega\tau + \Phi(\tau)\right] \tag{15}$$

where A and Φ are presumed to be slowly varying functions of τ. When this expression for ζ_c is substituted into equation (14) and the appropriate averages are carried out, two equations result (see appendix C).

$$\left(1 - \Omega^2\right)\bar{A} - \frac{\epsilon\Omega^2\bar{A}^3}{4} = G_n \cos \bar{\Phi} \tag{16a}$$

$$-2\beta_c\Omega\bar{A} = G_n \sin \bar{\Phi} \tag{16b}$$

Here $\bar{A}$ and $\bar{\Phi}$ are average values (over one period) of $A(\tau)$ and $\Phi(\tau)$. Squaring and adding equations (16) results in one equation involving $\bar{A}$:

$$\left[\left(1 - \Omega^2\right)\bar{A} - \frac{\epsilon\Omega^2\bar{A}^3}{4}\right]^2 + 4\beta_c{}^2\Omega^2\bar{A}^2 = G_n{}^2 \tag{17}$$

For given values of G_n, ϵ, β_c, and Ω, equation (17) can be used to compute $\bar{A}$. Then equation (16b) can be solved for $\bar{\Phi}$, and the approximate solution to equations (12) becomes

$$\zeta_c(\tau) = \bar{A} \cos(\Omega\tau + \bar{\Phi}) \tag{18a}$$

$$\zeta_s(\tau) = 0 \tag{18b}$$

for vibrations where only one bending mode $\left(\cos \frac{ny}{R}\right)$ responds. A typical resonance curve is shown in figure 2, which demonstrates the nonlinearity of the softening type.

The case of free vibrations may be obtained by putting G_n and β_c equal to zero in the preceding results. Equations (16) then yield

$$\Omega = 1 - \frac{\epsilon\bar{A}^2}{8} + O\left(\epsilon^2\right) \tag{19}$$

which is the so-called "backbone curve" for free nonlinear vibrations. This curve is illustrated in figure 3 for various values of ϵ.

Stability of the one-mode response.- The stability of the preceding solution was investigated by perturbing $\zeta_c(\tau)$ and $\zeta_s(\tau)$. A study of the resulting Mathieu equations indicates that within order ϵ^2

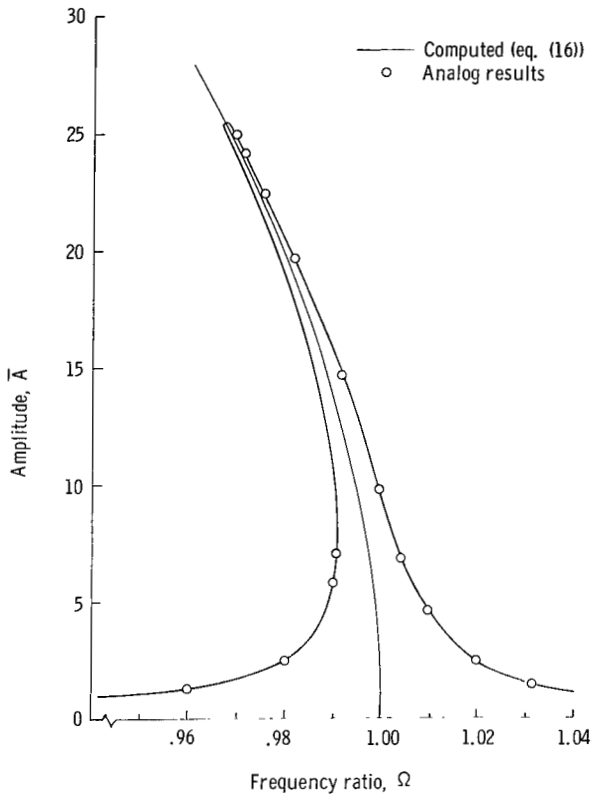

Figure 2.- Typical single-mode response. Driven mode, $\cos\frac{ny}{R}$. $\epsilon = 4.2 \times 10^{-4}$; $\beta_c = 2 \times 10^{-3}$; $G_n = 0.10$.

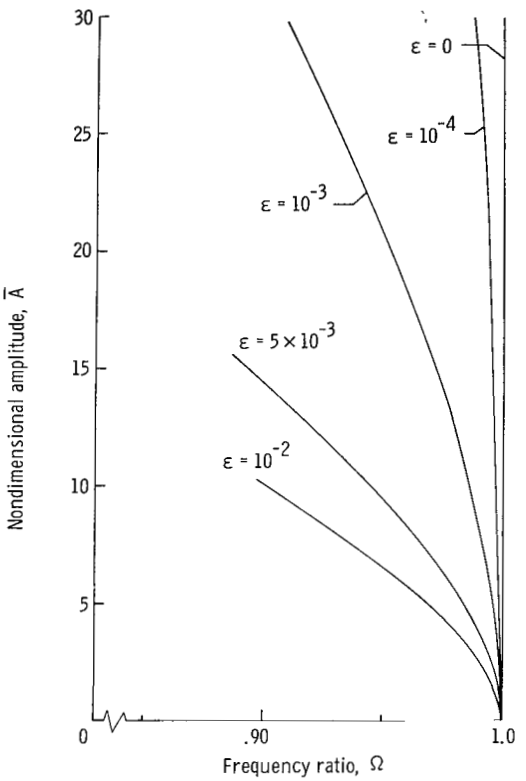

Figure 3.- Backbone curves for various values of ϵ. Nonlinearity parameter, $\epsilon = \left(\frac{n^2 h}{R}\right)^2$.

(1) perturbations of ζ_c are unstable within the area bounded by

$$1 - \frac{3\epsilon\bar{A}^2}{8} < \Omega < 1 - \frac{\epsilon\bar{A}^2}{8}$$

(2) perturbations of ζ_s are unstable within the region

$$1 - \frac{\epsilon\bar{A}^2}{8} < \Omega < 1 + \frac{\epsilon\bar{A}^2}{8}$$

(3) both types of perturbations are also unstable in narrow regions near $\Omega = \frac{1}{2}, \frac{1}{3}, \frac{1}{4}, \ldots$

Details of the stability calculations are given in appendix D, along with an interpretation of the stability boundaries. The results of the stability analysis (for the vibration of a single mode) are summarized in figure 4. In one region, the solution is unstable with respect to perturbations of ζ_c, and

jumps occur in the response. In an adjacent area, perturbations of ζ_s are unstable, and the companion mode begins to vibrate; this case of coupled vibrations is analyzed in the following section.

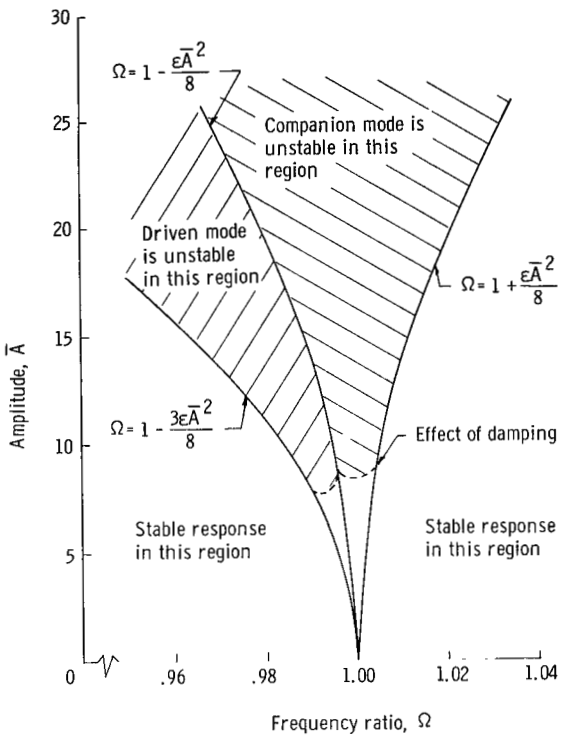

Figure 4.- Stability diagram for single-mode response.

Response of the self-coupled bending modes.- When $\zeta_s(\tau)$ and $\zeta_c(\tau)$ both oscillate, their coupled vibrations are governed by equations (12). As in the one-mode case, the method of averaging is employed to obtain approximate solutions. To use this method, let

$$\left.\begin{aligned}\zeta_c(\tau) &= A(\tau)\cos\left[\Omega\tau + \Phi(\tau)\right]\\ \zeta_s(\tau) &= B(\tau)\sin\left[\Omega\tau + \psi(\tau)\right]\end{aligned}\right\} \qquad (20)$$

where A, B, Φ, and ψ are presumed to to be slowly varying functions of τ.

Substituting the expressions for ζ_c and ζ_s from equations (20) into equations (12) and applying the method of averaging gives

$$\left(1 - \Omega^2\right)\bar{A} - 2\Omega\bar{A}\frac{d\Phi}{d\tau} - \frac{\epsilon\bar{A}}{4}\left[\Omega^2\bar{A}^2 + \frac{3}{2}\Omega\bar{A}^2\frac{d\Phi}{d\tau} - \Omega^2\bar{B}^2\cos 2\bar{\Delta} - \frac{\Omega\bar{B}}{2}\frac{d\bar{B}}{d\tau}\sin 2\bar{\Delta}\right.$$

$$\left. + \Omega\bar{B}^2\left(1 - \frac{1}{2}\cos 2\bar{\Delta}\right)\frac{d\bar{\psi}}{d\tau}\right] = G_n\cos\bar{\Phi} \qquad (21a)$$

$$-2\Omega\frac{d\bar{A}}{d\tau} - 2\Omega\beta_c\bar{A} - \frac{\epsilon\bar{A}}{4}\left(\frac{\Omega\bar{A}}{2}\frac{d\bar{A}}{d\tau} + \Omega^2\bar{B}^2\sin 2\bar{\Delta} - \frac{\Omega\bar{B}}{2}\cos 2\bar{\Delta}\frac{d\bar{B}}{d\tau}\right.$$

$$\left. + \frac{\Omega\bar{B}^2}{2}\sin 2\bar{\Delta}\frac{d\bar{\psi}}{d\tau}\right) = G_n\sin\bar{\Phi} \qquad (21b)$$

$$\left(1 - \Omega^2\right)\bar{B} - 2\Omega\bar{B}\frac{d\bar{\psi}}{d\tau} - \frac{\epsilon\bar{B}}{4}\left[-\Omega^2\bar{A}^2\cos 2\bar{\Delta} + \Omega^2\bar{B}^2 + \Omega\bar{A}^2\left(1 - \frac{1}{2}\cos 2\bar{\Delta}\right)\frac{d\bar{\Phi}}{d\tau}\right.$$

$$\left. + \frac{\Omega\bar{A}}{2}\sin 2\bar{\Delta}\frac{d\bar{A}}{d\tau} + \frac{3}{2}\Omega\bar{B}^2\frac{d\bar{\psi}}{d\tau}\right] = 0 \qquad (21c)$$

$$2\Omega \frac{d\bar{B}}{d\tau} + 2\beta_s \Omega \bar{B} - \frac{\epsilon \bar{B}}{4}\left(\Omega^2 \bar{A}^2 \sin 2\bar{\Delta} - \frac{\Omega \bar{B}}{2} \frac{d\bar{B}}{d\tau}\right.$$

$$\left. + \frac{\Omega \bar{A}}{2} \cos 2\bar{\Delta} \frac{d\bar{A}}{d\tau} + \frac{\Omega \bar{A}^2}{2} \sin 2\bar{\Delta} \frac{d\bar{\Phi}}{d\tau}\right) = 0 \qquad (21d)$$

where $A(\tau)$, $B(\tau)$, $\Phi(\tau)$, and $\psi(\tau)$ have been replaced by their average values over one cycle and are denoted by $\bar{A}$, $\bar{B}$, $\bar{\Phi}$, and $\bar{\psi}$. The average phase difference $\bar{\Delta}$ is

$$\bar{\Delta} = \bar{\psi} - \bar{\Phi} \qquad (22)$$

For steady-state vibrations, the average values $\bar{A}$, $\bar{B}$, $\bar{\Phi}$, and $\bar{\psi}$ are all constant; in this case, their time derivatives ($d\bar{A}/d\tau$, $d\bar{B}/d\tau$, etc.) are all zero, and equations (21) reduce to

$$\left(1 - \Omega^2\right)\bar{A} - \frac{\epsilon \Omega^2 \bar{A}}{4}\left(\bar{A}^2 - \bar{B}^2 \cos 2\bar{\Delta}\right) = G_n \cos \bar{\Phi} \qquad (23a)$$

$$-2\beta_c \Omega \bar{A} - \frac{\epsilon \Omega^2 \bar{A}}{4} \bar{B}^2 \sin 2\bar{\Delta} = G_n \sin \bar{\Phi} \qquad (23b)$$

$$\left(1 - \Omega^2\right)\bar{B} - \frac{\epsilon \Omega^2 \bar{B}}{4}\left(\bar{B}^2 - \bar{A}^2 \cos 2\bar{\Delta}\right) = 0 \qquad (23c)$$

$$2\beta_s \Omega \bar{B} - \frac{\epsilon \Omega^2 \bar{B}}{4} \bar{A}^2 \sin 2\bar{\Delta} = 0 \qquad (23d)$$

Equations (23) may be solved simultaneously for $\bar{A}$, $\bar{B}$, $\bar{\Phi}$, and $\bar{\psi}$, and the approximate solution to equations (12) then becomes

$$\zeta_c(\tau) = \bar{A} \cos(\Omega\tau + \bar{\Phi}) \qquad (24a)$$

$$\zeta_s(\tau) = \bar{B} \sin(\Omega\tau + \bar{\psi}) \qquad (24b)$$

Details of the calculations are given in appendix E. Response curves of the variation of $\bar{A}$ with Ω and $\bar{B}$ with Ω are shown in figure 5, where the particular values

$$G_n = 0.1 \quad (\text{Force} = G_n \cos \Omega\tau)$$

$$\beta_c = \beta_s = 2 \times 10^{-3} \quad (\text{Viscous damping})$$

and

$$\epsilon = \left(\frac{n^2 h}{R}\right)^2 = 4.2 \times 10^{-4} \quad \text{(Nonlinearity parameter)}$$

were used.

A surprising feature of the two-mode response was the appearance of a "gap," or discontinuity in the solution. Slightly to the left of the resonance peak in figure 5, the approximate solutions for ζ_c and ζ_s break down. The results of a subsequent stability analysis showed that the gap in the response coincides with a narrow region in which both the one-mode solution (eqs. (18)) and the two-mode solution (eqs. (24)) are unstable. The experiments suggest that a "beating" response exists in this area, with the ring vibrating first in one mode, then in two modes, then back to one, and so forth.

Analog-computer studies (discussed in a subsequent section) verified the calculated response curves, and nonsteady vibrations were found to occur in the gap region. Similar responses involving gaps have been observed in the case of fuel sloshing and in other nonlinear problems. (See refs. 22 and 23.)

Another curious result demonstrated in figure 5 is that in some cases the companion mode $\left(\sin \frac{ny}{R}\right.$, which is not driven by the forcing function$\left.\right)$ can vibrate to larger amplitudes than the driven mode $\left(\cos \frac{ny}{R}\right)$. Responses of this type occur for $\Omega < 1$ and were detected experimentally.

It will also be noted that in the two-mode case the amplitude of the driven mode is considerably reduced from what it would be if $\sin \frac{ny}{R}$ did not vibrate. A comparison of the driven-mode response for both cases (one mode and two modes) is shown in figure 6.

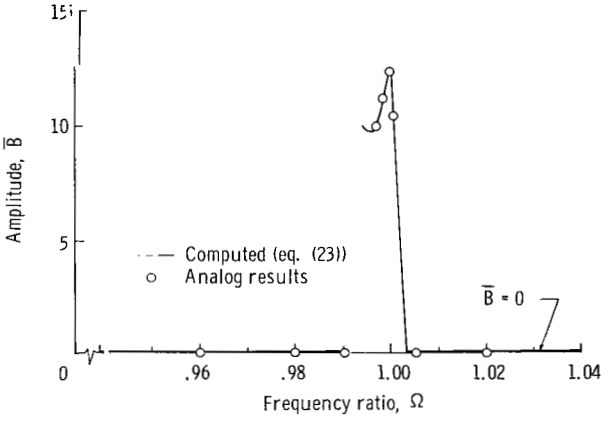

(a) Companion mode, $\sin \frac{ny}{R}$.

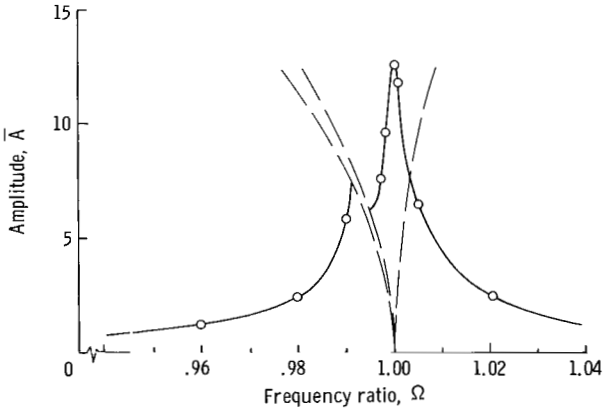

(b) Driven mode, $\cos \frac{ny}{R}$.

Figure 5.- Typical coupled-mode response. $\epsilon = 4.2 \times 10^{-4}$; $\beta_c = \beta_s = 2 \times 10^{-3}$; $G_n = 0.10$.

Finally, both figures 5 and 6 show that the two-mode response is almost linear, at least in those areas where the vibrations are stable.

Stability of the coupled-mode response.- As for the one-mode case, the stability of the coupled-mode vibrations can be found by perturbing the steady-state response. The resulting analysis shows that within order ϵ^2 real non-zero values of $\bar{B}$ do not exist for

$$\Omega > 1 + \frac{\epsilon \bar{A}^2}{8}$$

and the two-mode solution is unstable for

$$\Omega < 1 - \frac{2.38 \epsilon \bar{A}^2}{8}$$

These results are presented in figure 7, and the corresponding stability calculations are outlined in appendix F.

A comparison of the preceding results with the results for the unstable regions given previously shows that the one-mode and the two-mode solutions are both unstable in a narrow region given by

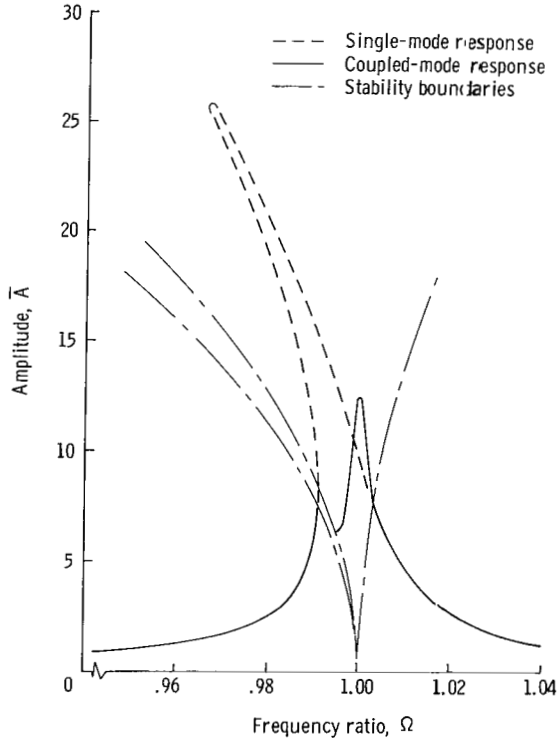

Figure 6.- Comparison of driven-mode response for one mode and two modes. $\epsilon = 4.2 \times 10^{-4}$; $\beta_c = \beta_s = 2 \times 10^{-3}$; $G_n = 0.10$.

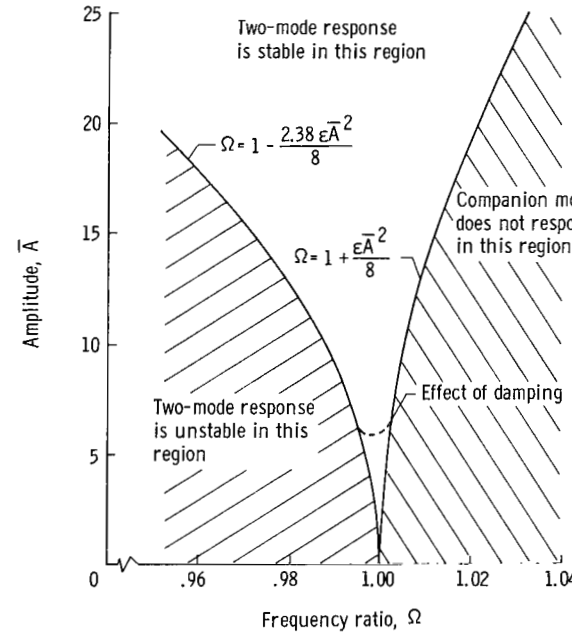

Figure 7.- Stability diagram for coupled-mode response.

$$1 - \frac{3\epsilon\bar{A}^2}{8} < \Omega < 1 - \frac{2.38\epsilon\bar{A}^2}{8}$$

As noted previously, this region coincides with the gap in the two-mode response. The gap in the solution is apparently caused when the assumption of slowly varying amplitudes and phases inherent in the theory no longer applies to the actual motions of the ring.

This discussion concludes the one- and two-mode analysis in this report. The calculations can be extended to account for the effect of tangential inertia and additional nonlinear terms which have been previously neglected. The general case, involving an infinite number of bending modes, has also been analyzed. (See ref. 15.) These investigations indicate that the basic features of the vibrations are adequately given by the one- and two-mode study just presented. The results of the more refined approaches are briefly outlined in the following section; details of the calculations may be found in reference 15.

Improvements in the Analysis

Throughout the present study, many simplifying approximations have been used. In order to determine when these approximations are valid and when they break down, it is necessary to consider some refinements in the analysis. These refinements yield significant improvements in the theory and bring it in closer agreement with the experiments.

Discussion of tangential inertia and other effects.- Since the effect of tangential inertia has been neglected, equation (6) yields a slightly inaccurate result for the linear vibration frequency. Including the tangential inertia term (eq. (1a)) corrects this discrepancy, and repeating the analysis gives results in the form of equations (16) and (19), where Ω is replaced by

$$\frac{\omega}{\omega_L} = \frac{\text{Frequency of vibration}}{\text{Linear vibration frequency}}$$

and ϵ is replaced by

$$\epsilon_1 = \left(\frac{n^2}{n^2 + 1}\right)\left(1 + \frac{1}{8n^2}\right)\epsilon \tag{25}$$

In other words, the form of the results is unchanged, but the parameters Ω and ϵ are altered to account for the tangential inertia.

Other small corrections, such as those due to shear deformation, are generally unimportant if the ring is sufficiently thin. For instance, Buckens (ref. 8) has shown that shear deformation and rotary inertia may be neglected if

$$\frac{n^2h^2}{3R} \ll 1$$

This result is in agreement with the analogous result for beams - namely, that shear effects can be neglected if the $(\text{depth/length})^2$ ratio is much less than unity.

Similarly, the effect of extension of the midsurface of the ring is usually unimportant for bending vibrations of thin rings. This result is well established for linear vibrations (see ref's. 6, 8, and 12) and carries over in the nonlinear case as well (see ref. 15 in this regard).

Corrections for additional nonlinearities.- The preceding corrections are all relatively minor, and their influence is fairly well predicted on the basis of linear vibrations. A major improvement in the nonlinear analysis can be obtained when additional nonlinear terms are included in the strain-displacement relations. Up to this point, the calculations have all employed the usual nonlinear expression for the midplane circumferential strain, namely,

$$\epsilon_{yy}\Big|_{z=0} = \frac{\partial v}{\partial y} + \frac{w}{R} + \frac{1}{2}\left(\frac{\partial w}{\partial y}\right)^2 \tag{26a}$$

which is commonly used in nonlinear shell studies (e.g., refs. 1 to 4). However, equation (26a) is an approximation to the more complete strain-displacement relation (ref. 24)

$$\epsilon_{yy}\Big|_{z=0} = \frac{\partial v}{\partial y} + \frac{w}{R} + \frac{1}{2}\left[\left(\frac{\partial w}{\partial y} - \frac{v}{R}\right)^2 + \left(\frac{w}{R} + \frac{\partial v}{\partial y}\right)^2\right] \tag{26b}$$

When the deflection $w(y,t)$ is assumed in the form (eq. (8))

$$w(y,t) = A_n(t)\cos\frac{ny}{R} + B_n(t)\sin\frac{ny}{R} + A_o(t)$$

and equation (26a) is used in the inextensionality condition, $A_o(t)$ is found to be (eq. (9))

$$A_o(t) = -\frac{n^2}{4R}\left[A_n^2(t) + B_n^2(t)\right]$$

Then the deflection is (eq. (10))

$$w(y,t) = A_n(t)\cos\frac{ny}{R} + B_n(t)\sin\frac{ny}{R} - \frac{n^2}{4R}\left[A_n^2(t) + B_n^2(t)\right]$$

and the coefficient $n^2/4R$ eventually becomes the nonlinearity parameter $\epsilon = \left(\frac{n^2 h}{R}\right)^2$. Thus, the coefficient of $\left[A_n^2(t) + B_n^2(t)\right]$ in the preceding expression for w influences all the previous results (e.g., the response curves, the backbone curve, and stability boundaries) by means of ϵ.

In a similar fashion, when the more exact equation (26b) is used in the inextensionality condition, a more accurate expression for $A_o(t)$ results (see ref. 15)

$$A_o(t) = -\frac{n^2}{4R}\left(1 - \frac{1}{n^2}\right)^2\left[A_n^2(t) + B_n^2(t)\right] + \text{Terms of order } \left(\frac{A_n}{R}\right)^3, \left(\frac{B_n}{R}\right)^3 \qquad (27)$$

If the higher order terms are neglected, the improved version of the deflection then becomes

$$w(y,t) = A_n(t)\cos\frac{ny}{R} + B_n(t)\sin\frac{ny}{R} - \frac{n^2}{4R}\left(1 - \frac{1}{n^2}\right)^2\left[A_n^2(t) + B_n^2(t)\right] \qquad (28)$$

Since this expression for w has exactly the same form as the one which was previously used (eq. (10)), the analytical results are altered only through the new coefficient of $\left[A_n^2(t) + B_n^2(t)\right]$. That is, the results of the previous calculations can be modified to account for the additional nonlinearities by replacing $\epsilon = \left(\frac{n^2 h}{R}\right)^2$ by

$$\left(\frac{n^2 h}{R}\right)^2\left(1 - \frac{1}{n^2}\right)^4$$

This correction can be combined with the one which accounts for tangential-inertia effects by first defining a corrected nonlinearity parameter ϵ_c

$$\epsilon_c = \left(\frac{n^2}{n^2 + 1}\right)\left(1 + \frac{1}{8n^2}\right)\left(1 - \frac{1}{n^2}\right)^4\epsilon \qquad (29)$$

Then all the previous analytical results (response curves, etc.) may be corrected for both the additional nonlinearities and tangential inertia by replacing Ω by ω/ω_L and ϵ by the expression for ϵ_c (eq. (29)). The corrections are most noticeable for low values of n, with the effect of the additional nonlinearities predominating. For example, when $n = 2$, ϵ_c is about one-fourth as large as ϵ (i.e., the nonlinearity is reduced by nearly a factor of 4). Values of ϵ_c/ϵ for various values of n are given in the following table:

Mode number, n	ϵ_c/ϵ
2	0.261
3	.571
4	.734
5	.820
10	.950

The bulk of the experimental results were obtained for the $n = 4$ mode, and the comparison of theory and experiment was made by using $\epsilon_c = 0.734\epsilon$. The experimental work is discussed in the following section.

EXPERIMENTS

Apparatus

A thin seamless copper ring was used in the experiments; it had a radius of 4 inches (10.16 cm), a thickness of 5.1×10^{-3} inch (0.013 cm), and a length in the axial direction of 0.988 inch (2.51 cm). The ring was supported by four very thin suspension threads, equally spaced around the circumference, as shown in figure 8.

Radial motions of the ring were measured by two inductance pickups which operated in a push-pull fashion. These deflection sensors were mounted on a fixture with a large bearing that allowed them to move circumferentially around the ring. Vibrations of the ring were excited by means of an electrodynamic shaker. The shaker was connected to the ring by a fine tungsten drive wire (0.001-inch (0.003-cm) diameter), which served as a very soft coupling spring between the shaker and the ring. (A simplified sketch of the apparatus is shown in fig. 8.) This arrangement made it possible to estimate the amplitude of the force which was experimentally applied to vibrate the ring.

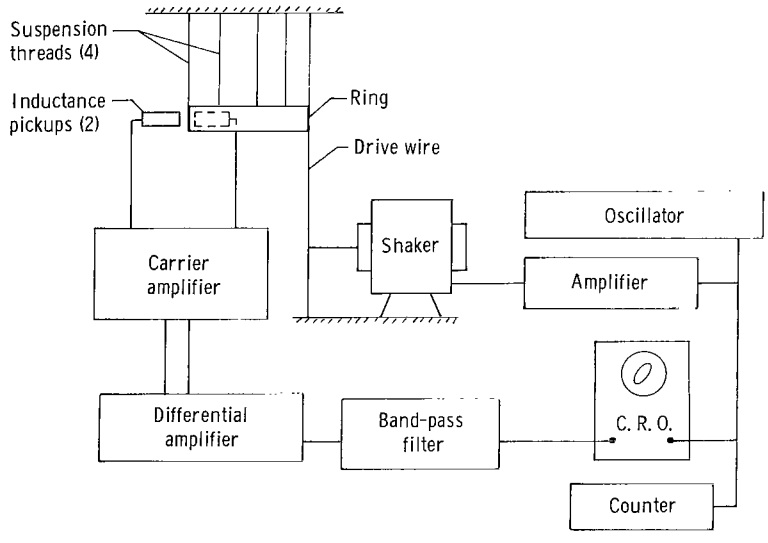

Figure 8.- Simplified schematic of experimental apparatus.

The response of the ring was analyzed, and the vibration modes were identified by means of Lissajous figures. These and other technical details of the experiments are discussed in appendix G.

Measurement of Mode Shapes

The mode shapes were measured by exciting one mode $\left(\cos \frac{ny}{R}, \quad n = 4\right)$ and recording the amplitude of the response at intervals along a half wavelength. Measurements were made separately on two different half waves; the amplitudes ranged from about 1 to 27 times the thickness of the ring. These amplitude measurements are shown in

figure 9, where the solid lines correspond to the deflection shape assumed in the analysis. As indicated in figure 9, the main vibration shape was virtually independent of amplitude. Additional results presented in reference 15 include a plot of the root-mean-square response around the circumference of the ring and measurement of the motions which occurred at the nodes of $\cos \frac{ny}{R}$ for the single-mode response.

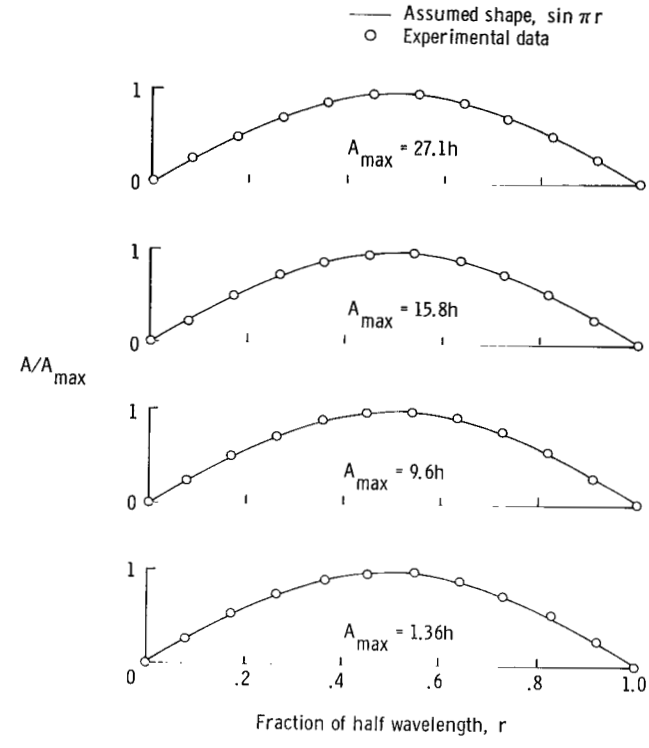

Figure 9.- Comparison of assumed mode shape and experimental results for various amplitudes.

Response Curves for the n = 4 Mode

Some typical experimental results are shown in nondimensional form in figure 10 for four different values of the input force. The magnitude of the input force was held constant for the individual response curves by maintaining a fixed displacement of the shaker ($2\delta_o$, peak-to-peak) during each run. An electronic counter was used to measure the period of the forcing function at each data point; by this procedure it was possible to determine the frequency ratio ω/ω_L very accurately. The amplitude of $A_n(t)$ was measured at one antinode of $\cos \frac{ny}{R}$, and the phase of the response Φ_A was determined there with a standard phase meter; the magnitude of $B_n(t)$ was measured at an adjacent node of $\cos \frac{ny}{R}$. To facilitate comparison with the analysis, these experimental amplitudes were nondimensionalized on the ring thickness.

Corresponding theoretical results are shown by the solid lines in figure 10. The backbone curves were calculated by using equation (19) with ω/ω_L in place of Ω and ϵ_c substituted for ϵ; both changes were made to account for the influence of tangential inertia and the additional nonlinearities discussed previously. The same corrections were used in computing the forced response, which was obtained from equations (16) for the undamped case. The input force used for these calculations was computed from the shaker displacement and the spring constant of the drive wire. A detailed comparison of the calculated and measured response for the driven mode is given in figure 11, which is for a peak-to-peak shaker displacement of $2\delta_o = 0.3$ inch (0.76 cm).

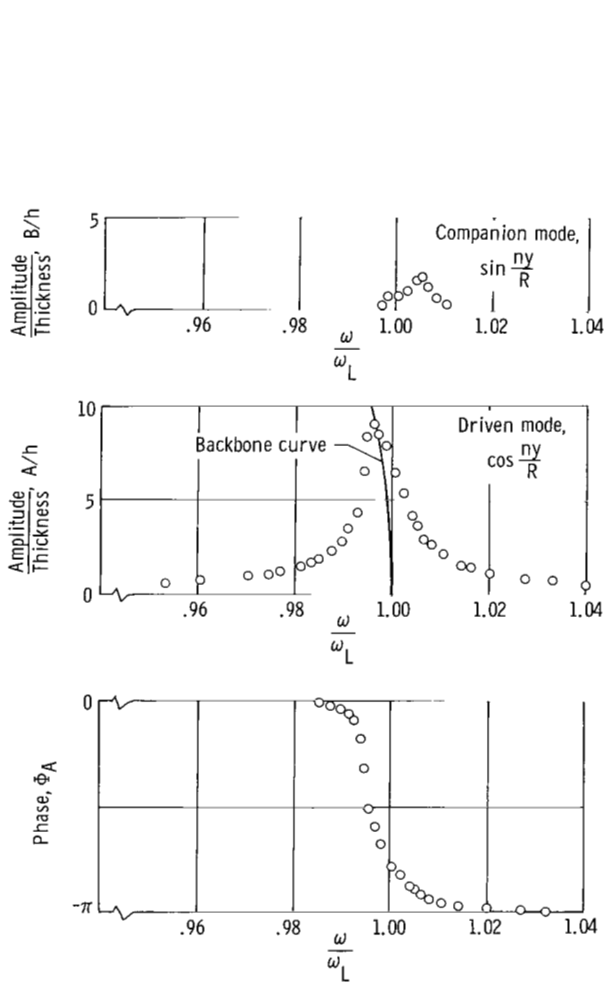

(a) Shaker displacement:
$2\delta_0$ = 0.100 in. (0.254 cm).

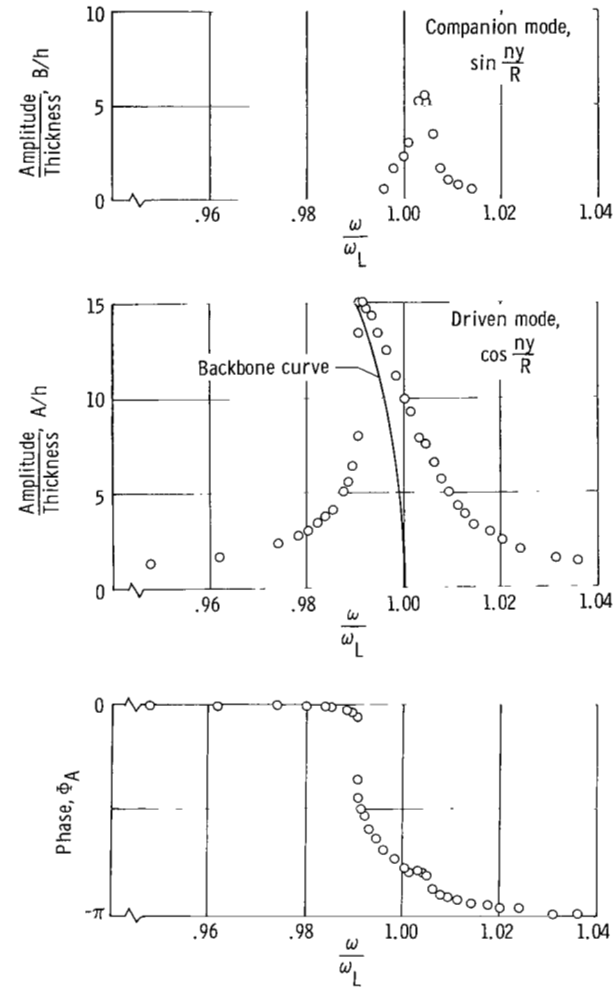

(b) Shaker displacement:
$2\delta_0$ = 0.200 in. (0.508 cm).

Figure 10.- Response curves for n = 4 mode.

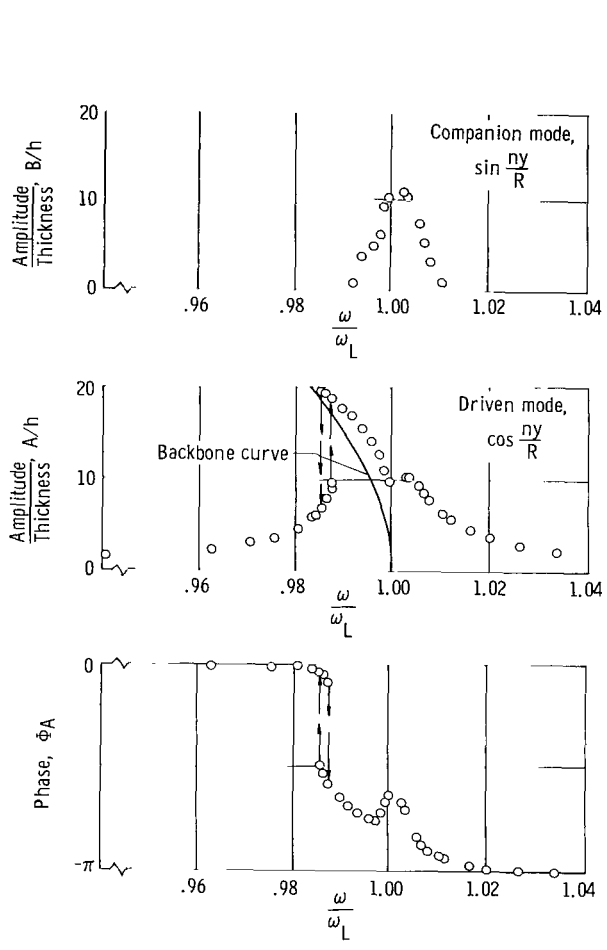

(c) Shaker displacement: $2\delta_0$ = 0.300 in. (0.762 cm).

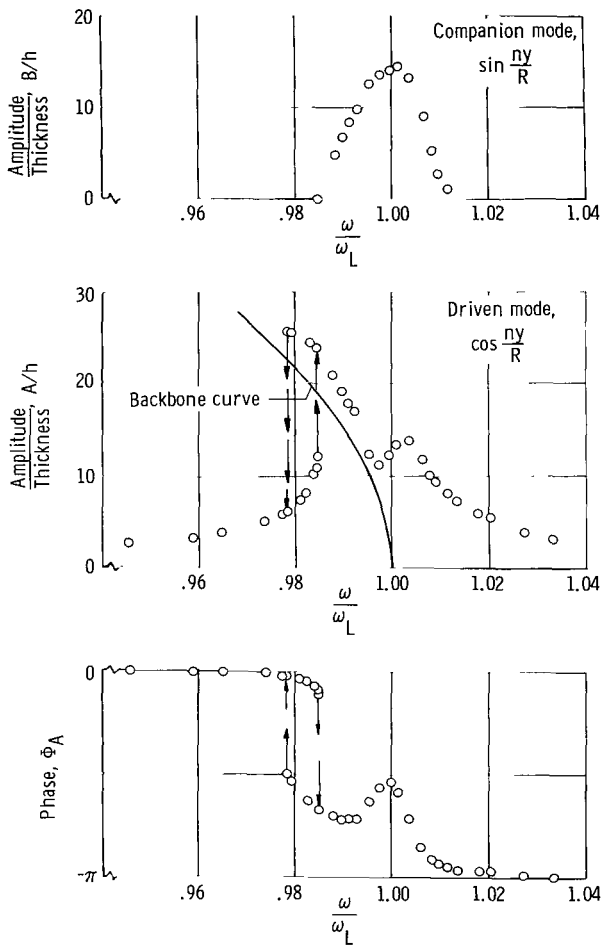

(d) Shaker displacement: $2\delta_0$ = 0.400 in. (1.016 cm).

Figure 10.- Concluded.

Discussion of the Experimental Results

As shown in figure 9, the experimentally determined mode shapes were nearly perfect sine waves along any half wavelength. This result was found to be independent of the maximum amplitude of the motion, as figure 9 indicates. For the single-mode response, the displacements at the nodes of $\cos \frac{ny}{R}$ were found to increase linearly with the square of the maximum amplitude. (See ref. 15.) This behavior is in agreement with the analytical results.

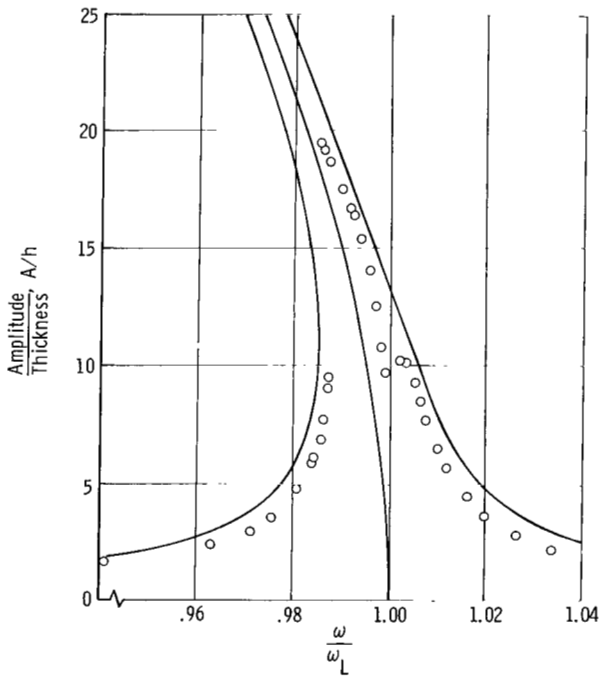

Figure 11.- Calculated and measured response. n = 4 mode; $2\delta_0$ = 0.300 in. (0.762 cm); $\varepsilon_c = 3.08 \times 10^{-4}$.

The response curves of figure 10 show good correlation with the theoretical backbone curves, and figure 11 shows a frequency difference of less than 1 percent between theory and experiment. This slight discrepancy was probably due to small errors in estimating the force applied to the ring.

The experimental response curves exhibited the jump phenomena and the appearance of a secondary resonance peak for the driven mode. The latter peak resulted from the fact that, in the experiment, the driven mode and the companion mode had slightly different natural frequencies. Because of this disparity, it was not possible to make a quantitative comparison of the coupled-mode response with the corresponding theory. However, qualitative agreement with the analysis was obtained for the two-mode case and included the result that in some instances the companion mode vibrated to larger amplitudes than the driven mode. One major feature of the theory which was not detected experimentally was the so-called "gap" in the response; the disappearance of the gap was apparently due to the difference in the natural frequencies of the coupled modes. The only results which might have been related to the gap were occasional nonsteady beating responses. These were sometimes observed to the left of the companion-mode resonance peak.

In order to understand more fully the response of the ring in the gap region and to verify that such a gap did theoretically exist, equations (12) were solved on an analog computer. The analog solutions confirmed the previous analytical results, as shown in figures 2 and 5. Nonsteady vibrations with beats occurred in the gap region. The analog procedure is outlined in appendix H.

CONCLUDING REMARKS

The nonlinear flexural vibrations of thin rings were analyzed by choosing vibration modes and applying Galerkin's procedure. The vibrations were assumed to involve no stretching of the midsurface of the ring; this assumption was found to be adequate for the study of flexural vibrations. In the analysis, only one mode was directly driven by the forcing function; nevertheless, it was necessary to include two vibration modes in the calculations because under certain conditions, nonlinear coupling caused the companion mode to respond and participate in the motion. In other cases, the single-mode response was sufficient.

Significant improvement in the theory was obtained by including the effect of additional nonlinearities in the strain-displacement relations. Retaining the effect of tangential inertia also improved the calculations, but to a lesser extent. Both these modifications lose their importance as the mode number increases; however, they combined to decrease the nonlinearity parameter by more than 25 percent for the third flexural mode ($n = 4$).

The experimental results were found to be in good agreement with the analysis, both qualitatively and quantitatively. Theory and experiment both exhibited the jump phenomenon, nonlinearity of the softening type, and the appearance of the companion mode. The measured responses were in good agreement with the calculated values, and the experimental mode shapes demonstrated the appropriateness of the deflection form employed in the analysis.

The results of the present study are characteristic of the nonlinear forced vibrations of axisymmetric elastic bodies. In such structures, the nonlinear forced vibration of one mode often results in the response of both the driven mode and its companion. Vibrations of this type occur because of the nonlinear coupling that exists between the modes involved. The nonlinear forced vibration of thin circular cylinders, thin circular cones, and other thin axisymmetric structures can be expected to exhibit similar behavior.

Langley Research Center,
National Aeronautics and Space Administration,
Langley Station, Hampton, Va., August 4, 1965.

APPENDIX A

CONVERSION OF U.S. CUSTOMARY UNITS TO SI UNITS

The International System of Units (SI) was adopted by the Eleventh General Conference on Weights and Measures, Paris, October 1960, in Resolution No. 12 (ref. 16). Conversion factors for the units used herein are given in the following table:

Physical quantity	U.S. Customary Unit	Conversion factor (*)	SI unit
Force	lb	4.45	newtons (N)
Frequency	cps	1	hertz (Hz)
Length	in.	0.0254	meter (m)
Load	lb/in^2	6895	$newton/meter^2$ (N/m^2)
Mass density	$lb\text{-}sec^2/in^4$	27 679.9	$kilogram/meter^3$ (kg/m^3)
Moment per unit length	in-lb/in.	4.45	meter-newton/meter (m-N/m)
Stiffness	lb/in.	175.2	newton/meter (N/m)
Young's modulus	lb/in^2	6895	$newton/meter^2$ (N/m^2)

*Multiply value given in U.S. Customary Unit by conversion factor to obtain equivalent value in SI unit.

Prefix to indicate multiple of units is as follows:

Prefix	Multiple
centi	10^{-2}

APPENDIX B

THE EQUATIONS OF MOTION

The equations of motion for a thin circular ring become nonlinear when finite displacements are considered. The purpose of this appendix is to present a brief development of these equations.

Useful Results From Shell Theory

The equations for rings can be obtained in a straightforward manner by a specialization of the analogous equations for thin cylinders. The latter equations have long been employed in nonlinear analyses of thin cylindrical shells; they are often derived (e.g., refs. 1 and 2) and are simply repeated here:

$$\frac{\partial N_x}{\partial x} + \frac{\partial N_{xy}}{\partial y} = \rho h \frac{\partial^2 u}{\partial t^2} \tag{B1}$$

$$\frac{\partial N_{xy}}{\partial x} + \frac{\partial N_y}{\partial y} = \rho h \frac{\partial^2 v}{\partial t^2} \tag{B2}$$

$$\frac{\partial^2 M_x}{\partial x^2} + 2 \frac{\partial^2 M_{xy}}{\partial x \, \partial y} + \frac{\partial^2 M_y}{\partial y^2} + \frac{\partial}{\partial x}\left(N_x \frac{\partial w}{\partial x} + N_{xy} \frac{\partial w}{\partial y}\right) + \frac{\partial}{\partial y}\left(N_y \frac{\partial w}{\partial y} + N_{xy} \frac{\partial w}{\partial x}\right)$$

$$- \frac{N_y}{R} + q(x,y,t) = \rho h \frac{\partial^2 w}{\partial t^2} \tag{B3}$$

The variables u, v, and w are the midplane displacements in the axial, circumferential, and radial directions, respectively. (See fig. 1.) Forces and moments per unit length (N_x, N_y, M_x, etc.), defined in terms of the stresses, are

$$\left.\begin{aligned} N_x &= \int_{-h/2}^{h/2} \sigma_{xx} \, dz \qquad N_{xy} = \int_{-h/2}^{h/2} \sigma_{xy} \, dz \qquad N_y = \int_{-h/2}^{h/2} \sigma_{yy} \, dz \\ M_x &= \int_{-h/2}^{h/2} \sigma_{xx} z \, dz \qquad M_{xy} = \int_{-h/2}^{h/2} \sigma_{xy} z \, dz \qquad M_y = \int_{-h/2}^{h/2} \sigma_{yy} z \, dz \end{aligned}\right\} \tag{B4}$$

The applied load $q(x,y,t)$ acts in the radial direction.

Equations (B1) to (B3) contain both forces and moments as well as displacements. Before specializing these equations to apply to rings, it is

desirable to express them in a more workable form. To achieve the desired form, the following procedure is used:

(1) The strains are related to the displacements u, v, and w

(2) Hooke's law is used to relate the stresses to the strains

(3) By combining the relations from (1) and (2), the stresses are written in terms of the displacements and then employed in equations (B1) to (B4).

The strain-displacement relations are approximated by

$$\left.\begin{aligned} \epsilon_{xx} &= \frac{\partial u}{\partial x} + \frac{1}{2}\left(\frac{\partial w}{\partial x}\right)^2 - z\,\frac{\partial^2 w}{\partial x^2} \\ \epsilon_{yy} &= \frac{\partial v}{\partial y} + \frac{w}{R} + \frac{1}{2}\left(\frac{\partial w}{\partial y}\right)^2 - z\,\frac{\partial^2 w}{\partial y^2} \\ \epsilon_{xy} &= \frac{\partial v}{\partial x} + \frac{\partial u}{\partial y} + \frac{\partial w}{\partial x}\,\frac{\partial w}{\partial y} - 2z\,\frac{\partial^2 w}{\partial x\,\partial y} \end{aligned}\right\} \tag{B5}$$

Transverse shear deformation is neglected, and the transverse normal stress is assumed to be negligible. These assumptions may be written as

$$\epsilon_{xz} = 0 \qquad \epsilon_{yz} = 0 \qquad \sigma_{zz} = 0$$

These relations are commonly employed in nonlinear analyses of thin cylinders. Terms like $\frac{1}{2}\left(\frac{\partial w}{\partial y}\right)^2$ give rise to nonlinearities in the equations of motion.

Next, Hooke's law is used to relate the stresses to the strains and with the preceding assumptions yields

$$\sigma_{yy} = \frac{E}{1 - \nu^2}\left(\epsilon_{yy} + \nu\epsilon_{xx}\right)$$

$$\sigma_{xx} = \frac{E}{1 - \nu^2}\left(\epsilon_{xx} + \nu\epsilon_{yy}\right)$$

$$\sigma_{xy} = \frac{E}{2(1 + \nu)}\,\epsilon_{xy}$$

where E is Young's modulus and ν is Poisson's ratio. Employing these stresses and equations (B5) in equations (B4) and carrying out the integration through the thickness gives the following forces and moments in terms of the displacements:

$$
\left.
\begin{aligned}
N_y &= \frac{Eh}{1 - \nu^2}\left\{\frac{\partial v}{\partial y} + \frac{w}{R} + \frac{1}{2}\left(\frac{\partial w}{\partial y}\right)^2 + \nu\left[\frac{\partial u}{\partial x} + \frac{1}{2}\left(\frac{\partial w}{\partial x}\right)^2\right]\right\} \\
N_x &= \frac{Eh}{1 - \nu^2}\left\{\frac{\partial u}{\partial x} + \frac{1}{2}\left(\frac{\partial w}{\partial x}\right)^2 + \nu\left[\frac{\partial v}{\partial y} + \frac{w}{R} + \frac{1}{2}\left(\frac{\partial w}{\partial y}\right)^2\right]\right\} \\
N_{xy} &= \frac{Eh}{2(1 + \nu)}\left(\frac{\partial v}{\partial x} + \frac{\partial u}{\partial y} + \frac{\partial w}{\partial x}\frac{\partial w}{\partial y}\right) \\
M_y &= -D\left(\frac{\partial^2 w}{\partial y^2} + \nu\frac{\partial^2 w}{\partial x^2}\right) \\
M_x &= -D\left(\frac{\partial^2 w}{\partial x^2} + \nu\frac{\partial^2 w}{\partial y^2}\right) \\
M_{xy} &= -D(1 - \nu)\frac{\partial^2 w}{\partial x\,\partial y}
\end{aligned}
\right\} \qquad (B6)
$$

where the bending stiffness $D = \frac{Eh^3}{12(1 - \nu^2)}$.

Derivation of Ring Equations

To specialize the cylinder equations to a ring, the following assumptions are made:

(1) The displacements w and v, as well as the radial load q, are taken to be functions of only the circumferential coordinate y and time t.

(2) The thickness and the width of the ring are both taken to be constant. The ring is assumed to be thin, so that $\left(\frac{h}{R}\right)^2$ is negligible in comparison with unity.

(3) The forces N_x and N_{xy} are assumed to be zero throughout the ring. The boundary conditions require that N_x and N_{xy} vanish at the ends of the ring (at $x = 0$, $x = b$ (fig. 1)); for flexural vibrations, rapid changes in the x-direction are not anticipated, and it becomes reasonable to assume that $N_x = 0$ and $N_{xy} = 0$ throughout the ring.

When these assumptions are used, equations (B6) reduce to

$$\left.\begin{aligned} N_y &= Eh\left[\frac{\partial v}{\partial y} + \frac{w}{R} + \frac{1}{2}\left(\frac{\partial w}{\partial y}\right)^2\right] \\ N_x &= 0 \\ N_{xy} &= 0 \\ M_y &= -D\,\frac{\partial^2 w}{\partial y^2} \\ M_x &= -\nu D\,\frac{\partial^2 w}{\partial y^2} \\ M_{xy} &= 0 \end{aligned}\right\} \tag{B7}$$

Substituting equations (B7) in equations (B1) to (B3) yields the following ring equations:

$$0 = \rho h\,\frac{\partial^2 u}{\partial t^2} \tag{B8}$$

$$\frac{\partial N_y}{\partial y} = \rho h\,\frac{\partial^2 v}{\partial t^2} \tag{B9}$$

$$D\,\frac{\partial^4 w}{\partial y^4} + \frac{N_y}{R} - \frac{\partial}{\partial y}\left(N_y\,\frac{\partial w}{\partial y}\right) + \rho h\,\frac{\partial^2 w}{\partial t^2} = q(y,t) \tag{B10}$$

where

$$N_y = Eh\left[\frac{\partial v}{\partial y} + \frac{w}{R} + \frac{1}{2}\left(\frac{\partial w}{\partial y}\right)^2\right] \tag{B11}$$

Equation (B8) is unimportant for the problems dealt with herein and will henceforth be dropped.

Note that there is a similarity between equations (B9) and (B10) and the following analogous equations for a vibrating beam:

$$\frac{\partial T}{\partial x} = \rho S\,\frac{\partial^2 v}{\partial t^2} \tag{B12}$$

$$EI \frac{\partial^4 w}{\partial x^4} - \frac{\partial}{\partial x}\left(T \frac{\partial w}{\partial x}\right) + \rho S \frac{\partial^2 w}{\partial t^2} = q(x,t) \qquad (B13)$$

where

S	cross-sectional area
T	longitudinal tension in beam
EI	bending stiffness
x	longitudinal coordinate
q	transverse load
w,v	lateral and longitudinal displacements, respectively

The term N_y/R occurs for the ring but not for the beam because the ring is curved.

It should be noted at this point that the ring equations (eqs. (B9) and (B10)) contain the same shortcomings inherent in the cylinder equations (eqs. (B1) to (B6)). For example, both sets of equations make the assumption that $1/n^2$ is negligible in comparison with unity (where n is the circumferential mode number). As a result, these equations lose their accuracy for low values of n (e.g., $n < 6$). In the case of cylinders, Morley (ref. 25) removed this difficulty by modifying the bending terms. This modification was accomplished by replacing $D\nabla^4 w$ by $D\left(\nabla^2 + \frac{1}{R^2}\right)^2 w$ in the final equations; the analogous modification of equations (B9) and (B10) results in the following set of improved equations of motion for a ring (eqs. (1a) and (1b)):

$$\frac{\partial N_y}{\partial y} = \rho h \frac{\partial^2 v}{\partial t^2}$$

$$D\left(\frac{\partial^2}{\partial y^2} + \frac{1}{R^2}\right)\left(\frac{\partial^2 w}{\partial y^2} + \frac{w}{R^2}\right) + \frac{N_y}{R} - \frac{\partial}{\partial y}\left(N_y \frac{\partial w}{\partial y}\right) + \rho h \frac{\partial^2 w}{\partial t^2} = q(y,t)$$

where

$$N_y = Eh\left[\frac{\partial v}{\partial y} + \frac{w}{R} + \frac{1}{2}\left(\frac{\partial w}{\partial y}\right)^2\right]$$

Except for the bending terms, equations (B9) and (B10) and (1a) and (1b) are identical. Because of this difference, however, only the latter set yields the correct linear ring vibration frequencies, and for this reason they are employed in the present analysis.

APPENDIX C

APPLICATION OF THE METHOD OF AVERAGING

The method of averaging (sometimes called "the method of slowly varying amplitude and phase") is often employed in nonlinear vibration problems. This technique is demonstrated here by applying it to equation (14) which is repeated here for convenience:

$$\frac{d^2\zeta_c}{d\tau^2} + 2\beta_c \frac{d\zeta_c}{d\tau} + \zeta_c + \frac{\epsilon\zeta_c}{2}\left[\zeta_c \frac{d^2\zeta_c}{d\tau^2} + \left(\frac{d\zeta_c}{d\tau}\right)^2\right] = G_n \cos \Omega\tau$$

To apply the method of averaging to this equation, let

$$\zeta_c(\tau) = A(\tau)\cos\left[\Omega\tau + \Phi(\tau)\right]$$

$$= A \cos \chi$$

where A and Φ are assumed to be slowly varying functions of τ, and χ designates $\left[\Omega\tau + \Phi(\tau)\right]$. Taking the derivative of $\zeta_c(\tau)$ gives

$$\frac{d\zeta_c}{d\tau} = -A\Omega \sin \chi + \frac{dA}{d\tau} \cos \chi - \frac{d\Phi}{d\tau} A \sin \chi \qquad (C1)$$

In the method of averaging, the result in equation (C1) is replaced by two equations; namely,

$$\frac{d\zeta_c}{d\tau} = -A\Omega \sin \chi \qquad (C2)$$

and

$$\frac{dA}{d\tau} \cos \chi - \frac{d\Phi}{d\tau} A \sin \chi = 0 \qquad (C3)$$

The second derivative $d^2\zeta_c/d\tau^2$ is then, computed from equation (C2),

$$\frac{d^2\zeta_c}{d\tau^2} = -A\Omega^2 \cos \chi - \frac{dA}{d\tau} \Omega \sin \chi - A \frac{d\Phi}{d\tau} \Omega \cos \chi \qquad (C4)$$

Next, the preceding approximations for ζ_c, $d\zeta_c/d\tau$, and $d^2\zeta_c/d\tau^2$ are substituted into equation (14). The result is

APPENDIX C

$$\left(1 - \Omega^2\right)A \cos \chi - \frac{dA}{d\tau} \Omega \sin \chi - A \frac{d\Phi}{d\tau} \Omega \cos \chi - 2\beta_c \Omega A \sin \chi$$

$$+ \frac{\epsilon}{2} A \cos \chi \left(-\Omega^2 A^2 \cos^2 \chi - \Omega A \frac{dA}{d\tau} \sin \chi \cos \chi - \Omega A^2 \frac{d\Phi}{d\tau} \cos^2 \chi\right.$$

$$\left. + \Omega^2 A^2 \sin^2 \chi\right) = G_n \cos(\chi - \Phi) \qquad (C5)$$

Both sides of equation (C5) are then multiplied by $\cos \chi$, and the result is added to equation (C3) after the latter has been multiplied by $\Omega \sin \chi$. This procedure yields

$$\left(1 - \Omega^2\right)A \cos^2 \chi - A\Omega \frac{d\Phi}{d\tau} - 2\beta_c \Omega A \sin \chi \cos \chi + \frac{\epsilon}{2} A \cos^2 \chi \left[-\Omega^2 A^2 \left(\cos^2 \chi - \sin^2 \chi\right)\right.$$

$$\left. -\Omega A \left(\frac{dA}{d\tau} \sin \chi \cos \chi + A \frac{d\Phi}{d\tau} \cos^2 \chi\right)\right] = G_n \left(\cos^2 \chi \cos \Phi + \sin \chi \cos \chi \sin \Phi\right) \qquad (C6)$$

Finally, this equation is "averaged" by integrating over one period on χ. In the integration, $A(\tau)$ and $\Phi(\tau)$ are approximated by their average values $\bar{A}$ and $\bar{\Phi}$, for example,

$$\int_0^{2\pi} A(\tau) \cos^2 \chi \, d\chi \approx \int_0^{2\pi} \bar{A} \cos^2 \chi \, d\chi = \bar{A}\pi$$

$$\int_0^{2\pi} A^3 \left(\frac{d\Phi}{d\tau}\right) \cos^4 \chi \, d\chi \approx \int_0^{2\pi} \bar{A}^3 \left(\frac{d\bar{\Phi}}{d\tau}\right) \cos^4 \chi \, d\chi = \frac{3\pi}{4} \bar{A}^3 \frac{d\bar{\Phi}}{d\tau}$$

where $d\bar{\Phi}/d\tau$ is the average value of $d\Phi/d\tau$. When equation (C6) is averaged in this fashion, it becomes

$$\left(1 - \Omega^2\right)\bar{A} - 2\Omega\bar{A} \frac{d\bar{\Phi}}{d\tau} - \frac{\epsilon\Omega^2 \bar{A}^3}{4} - \frac{3\epsilon\Omega\bar{A}^3}{8} \frac{d\bar{\Phi}}{d\tau} = G_n \cos \bar{\Phi} \qquad (C7)$$

In a similar fashion, a second equation for $\bar{A}$ and $\bar{\Phi}$ is obtained by

(1) Multiplying both sides of equation (C5) by $\sin \chi$

(2) Adding this result to equation (C3) after multiplying the latter by $-\Omega \cos \chi$

(3) Averaging the final equation by integrating both sides from $\chi = 0$ to 2π.

These manipulations give

$$-2\Omega \frac{d\bar{A}}{d\tau} - 2\beta_c \Omega \bar{A} - \frac{\epsilon \Omega \bar{A}^2}{8} \frac{d\bar{A}}{d\tau} = G_n \sin \bar{\Phi} \tag{C8}$$

Equations (C7) and (C8) are first-order coupled differential equations for $\bar{A}$ and $\bar{\Phi}$. They may be simplified to coupled algebraic equations when steady-state vibrations are considered. For example, steady-state vibrations imply that the average values $\bar{A}$ and $\bar{\Phi}$ remain steady (i.e., constant) with time. In this case, the average derivatives $d\bar{A}/d\tau$ and $d\bar{\Phi}/d\tau$ are identically zero, and equations (C7) and (C8) can be reduced to

$$\left(1 - \Omega^2\right)\bar{A} - \frac{\epsilon \Omega^2 \bar{A}^3}{4} = G_n \cos \bar{\Phi} \tag{16a}$$

$$-2\beta_c \Omega \bar{A} = G_n \sin \bar{\Phi} \tag{16b}$$

These algebraic equations can now be solved simultaneously to give $\bar{A}$ and $\bar{\Phi}$ as functions of G_n, ϵ, β_c, and Ω. Such a result is indicated in equation (17).

APPENDIX D

STABILITY OF THE ONE-MODE RESPONSE

To investigate the stability of the one-mode response (eqs. (18)), both $\zeta_c(\tau)$ and $\zeta_s(\tau)$ are disturbed slightly. The disturbed variables can be expressed as

$$\zeta_c(\tau) = \bar{A} \cos\left(\Omega\tau + \bar{\Phi}\right) + \xi_c(\tau) \tag{D1}$$

$$\zeta_s(\tau) = 0 + \xi_s(\tau) \tag{D2}$$

where $\xi_c(\tau)$ and $\xi_s(\tau)$ represent small perturbations in the response of $\cos\frac{ny}{R}$ and $\sin\frac{ny}{R}$, respectively. The solution (eqs. (18)) is said to be stable if ξ_c and ξ_s do not increase with time.

Substituting equations (D1) and (D2) for ζ_c and ζ_s into equations (12) and retaining only first-order terms in the perturbations gives

$$\left[1 + \frac{\epsilon\bar{A}^2}{2}\cos^2(\Omega\tau + \bar{\Phi})\right]\frac{d^2\xi_c}{d\tau^2} - \frac{\epsilon\bar{A}^2}{2}\sin 2(\Omega\tau + \bar{\Phi})\frac{d\xi_c}{d\tau}$$

$$+ \left\{1 + \frac{\epsilon\bar{A}^2}{2}\left[\sin^2(\Omega\tau + \bar{\Phi}) - 2\cos^2(\Omega\tau + \bar{\Phi})\right]\right\}\xi_c = 0 \tag{D3}$$

and

$$\frac{d^2\xi_s}{d\tau^2} + \left[1 - \frac{\epsilon\Omega^2\bar{A}^2}{2}\cos 2(\Omega\tau + \bar{\Phi})\right]\xi_c = 0 \tag{D4}$$

where $\bar{A}\cos(\Omega\tau + \bar{\Phi})$ is presumed to satisfy equation (14), and, for simplicity, the case $\beta_c = \beta_s = 0$ has been considered. (The case of nonzero damping is analyzed in ref. 15.)

Analysis of Perturbation Equations

It will be noted that equations (D3) and (D4) are ordinary differential equations with coefficients that are periodic in time. Such equations arise frequently in stability analyses; they are typified by the Mathieu equation,

$$\frac{d^2Y}{dZ^2} + (K + 16Q\cos 2Z)Y = 0 \tag{D5}$$

which has been studied extensively. (See refs. 21 and 26.) Its solutions are stable (bounded) for particular combinations of K and Q and unstable (unbounded) for others. Thus, associated with equation (D5) are certain stable and unstable regions in the KQ-plane. As indicated in the following paragraphs, the Mathieu equation results are useful in analyzing equations (D3) and (D4).

As it stands, equation (D3) has a periodic coefficient in every term. In simplified notation, it can be written as

$$\left(1 + \mu \cos^2\chi\right)\frac{d^2\xi_c}{d\tau^2} - \mu\Omega \sin 2\chi \frac{d\xi_c}{d\tau} + \left[1 + \mu\left(\sin^2\chi - 2\cos^2\chi\right)\right]\xi_c = 0 \qquad \text{(D6)}$$

where $\mu = \frac{\epsilon\bar{A}^2}{2}$ and $\chi = (\Omega\tau + \bar{\Phi})$.

The first-derivative term can be removed by using the following transformation of variables:

$$\left.\begin{aligned} \chi &= (\Omega\tau + \bar{\Phi}) \\ \frac{d}{d\tau} &= \frac{d}{d\chi}\frac{d\chi}{d\tau} \\ &= \Omega \frac{d}{d\chi} \\ \xi_c(\chi) &= U(\chi)e^{\int_0^\chi \frac{\mu \sin 2\chi d\chi}{2(1+\mu\cos^2\chi)}} \\ &= U(\chi)\left(1 + \mu \cos^2\chi\right) \end{aligned}\right\} \qquad \text{(D7)}$$

With these new variables, equation (D6) becomes

$$\left(1 + \mu \cos^2\chi\right)\frac{d^2U}{d\chi^2} + \left[\frac{1}{\Omega^2} + \mu\left(\sin^2\chi - 2\cos^2\chi\right) + \mu \cos 2\chi + \frac{\mu^2 \sin^2 2\chi}{4\left(1 + \mu \cos^2\chi\right)}\right]U = 0 \qquad \text{(D8)}$$

Dividing by $\left(1 + \mu \cos^2\chi\right)$ and expanding equation (D8) for small values of μ gives the approximate Mathieu equation

$$\frac{d^2U}{d\chi^2} + \frac{1}{\Omega^2}\left\{\left[1 - \frac{\epsilon\bar{A}^2}{4}\left(\Omega^2 + 1\right)\right] - \frac{\epsilon\bar{A}^2}{4}\left(\Omega^2 + 1\right)\cos 2\chi + O\left(\epsilon^2\right)\right\}U = 0 \qquad \text{(D9)}$$

where μ has been replaced by its equivalent $\frac{\epsilon\bar{A}^2}{2}$.

APPENDIX D

The first instability region of equation (D9) can be estimated from the known results for equation (D5). In terms of $\bar{A}$ and Ω, the one-mode response is unstable (with respect to perturbations of ζ_c) within the area bounded by

$$1 - \frac{3\epsilon\bar{A}^2}{8} + O(\epsilon^2) < \Omega < 1 - \frac{\epsilon\bar{A}^2}{8} + O(\epsilon^2)$$

The boundaries of this region coincide with the locus of vertical tangents to the response curves, where the jump phenomenon of nonlinear vibrations occurs.

In a similar fashion, the substitution $X = (\Omega\tau + \bar{\Phi})$ transforms equation (D4) to

$$\frac{d^2\xi_s}{dX^2} + \left(\frac{1}{\Omega^2} - \frac{\epsilon\bar{A}^2}{2}\cos 2X\right)\xi_s = 0 \qquad \text{(D10)}$$

The first instability region of this equation defines another area in which the one-mode response is not stable. In terms of the amplitude $\bar{A}$, instability of the solution requires that

$$\bar{A}^2 > \frac{4(\Omega^2 - 1)}{\epsilon\Omega^2} \qquad \text{for } \Omega \geqq 1$$

or

$$\bar{A}^2 > \frac{4(1 - \Omega^2)}{\epsilon\Omega^2} \qquad \text{for } \Omega \leqq 1$$

These inequalities may be expressed as a restriction on Ω, and the solution is unstable (with respect to perturbations in ζ_s) within the region

$$1 - \frac{\epsilon\bar{A}^2}{8} + O(\epsilon^2) < \Omega < 1 + \frac{\epsilon\bar{A}^2}{8} + O(\epsilon^2)$$

From a physical standpoint, the preceding conditions define a "critical amplitude" $\bar{A}_{cr}$ of the single-mode response. To understand this result more fully, recall that $\zeta_c(\tau)$ is associated with $\cos\frac{ny}{R}$ and that $\zeta_s(\tau)$ is related to $\sin\frac{ny}{R}$. The loading $q(y,t)$ was chosen so that the driven mode $\cos\frac{ny}{R}$ receives excitation from the external force and the $\sin\frac{ny}{R}$ mode receives none. This difference in excitation shows up in the differential equations which govern ζ_c and ζ_s, and a possible solution to these equations is

$$\zeta_c(\tau) = \bar{A}\cos(\Omega\tau + \bar{\Phi})$$

$$\zeta_s(\tau) = 0$$

where the $\sin \frac{ny}{R}$ mode does not vibrate. As pointed out by the stability analysis, however, if the driven mode exceeds the critical amplitude

$$\bar{A}_{cr} = \left(\frac{4\left|1 - \Omega^2\right|}{\epsilon \Omega^2} \right)^{1/2}$$

then the one-mode approximate solution becomes unstable. For amplitudes of $\cos \frac{ny}{R}$ in excess of $\bar{A}_{cr}$, the companion mode will respond, despite the fact that it is not (directly) excited by the forcing function.

Discussion of Stability Boundaries

The first instability region and the response of the companion mode have a simple physical explanation. The $\cos \frac{ny}{R}$ and $\sin \frac{ny}{R}$ modes may be regarded as the only modes of vibration of a two-degree-of-freedom system, where both modes have the same natural frequency. As a result of the nonlinear terms in the equations of motion, dynamic coupling exists between the modes. When one mode $\cos \frac{ny}{R}$ is harmonically excited in the vicinity of its natural frequency, the dynamic coupling causes the companion mode to respond. (In the terminology of nonlinear vibrations, the companion mode is said to be "parametrically excited.") Many other vibration problems give rise to similar coupled-mode vibrations; one such example is the nonlinear sloshing of liquid in circular tanks.

Up to this point, only the first (and most important) instability region has been discussed. The second, third, and higher instability regions of equations (D9) and (D10) indicate that the solution (eqs. (18)) becomes unstable in narrow areas near $\Omega = 1/2, 1/3, 1/4, \ldots$. Additional calculations are required to provide adequate solutions in these regions; such results are discussed on pages 54 to 56 in reference 15 under the title "Ultra-Harmonic Response." (For a general discussion of ultraharmonic responses, stability of vibrations, and jump behavior, see ref. 26.)

The results of the stability analysis for the one-mode response are summarized in figure 4, where the qualitative effect of damping is indicated by the dashed lines. Damping affects the stability boundaries primarily near $\Omega = 1$ and for small values of $\bar{A}$.

APPENDIX E

CALCULATION OF $\bar{A}$, $\bar{B}$, $\bar{\Phi}$, AND $\bar{\psi}$

Equations (22) and (23) form a set of five algebraic equations for $\bar{A}$, $\bar{B}$, $\bar{\Phi}$, $\bar{\Delta}$, and $\bar{\psi}$. From these equations, it is desirable to obtain response curves of the variations of $\bar{A}$, $\bar{B}$, $\bar{\Phi}$, and $\bar{\psi}$ with Ω for constant values of β_c, β_s, ϵ, and G_n. These results are best obtained by using an indirect approach, as is frequently the case in nonlinear problems.

The technique used was to treat G_n as an unknown and compute $\bar{B}$, G_n, $\bar{\Phi}$, and $\bar{\psi}$ for several values of $\bar{A}$ at particular values of Ω. This procedure resulted in curves of G_n plotted against $\bar{A}$ with Ω as a parameter. Then response curves of the variation of $\bar{A}$ with Ω for constant values of G_n were obtained by cross plotting. In a similar fashion, curves of $\bar{B}$ plotted against Ω, $\bar{\Phi}$ plotted against Ω, and so forth, were determined. The method is outlined in the following section. Note that in this approach $\bar{A}$ and Ω are regarded as being given, with $\bar{B}$, G_n, $\bar{\Phi}$, $\bar{\Delta}$, and $\bar{\psi}$ the unknowns.

To compute G_n, it was first necessary to represent $\sin 2\bar{\Delta}$, $\cos 2\bar{\Delta}$, and $\bar{B}^2$ in terms of known quantities by manipulating equations (23c) and (23d). For example, when $\bar{B}$ is nonzero, these equations become

$$\cos 2\bar{\Delta} = \frac{\bar{B}^2}{\bar{A}^2} + \frac{4\left(\Omega^2 - 1\right)}{\epsilon\Omega^2\bar{A}^2} \tag{E1}$$

and

$$\sin 2\bar{\Delta} = \frac{8\beta_s\Omega}{\epsilon\Omega^2\bar{A}^2} \tag{E2}$$

respectively. By using the identity $\sin^2 2\bar{\Delta} + \cos^2 2\bar{\Delta} = 1$, these equations combine to give a quadratic for $\bar{B}^2$:

$$\bar{B}^4 + \frac{8\left(\Omega^2 - 1\right)}{\epsilon\Omega^2}\bar{B}^2 + \frac{16\left(\Omega^2 - 1\right)^2 + \left(8\beta_s\Omega\right)^2 - \left(\epsilon\Omega^2\bar{A}^2\right)^2}{\left(\epsilon\Omega^2\right)^2} = 0$$

Solving this equation yields two roots for $\bar{B}^2$. In the present problem, the relevant expression is

$$\bar{B}^2 = \frac{4\left(1 - \Omega^2\right)}{\epsilon\Omega^2} + \frac{1}{\epsilon\Omega^2}\left[\left(\epsilon\Omega^2\bar{A}^2\right)^2 - \left(8\beta_s\Omega\right)^2\right]^{1/2} \tag{E3}$$

The other root is similar in form but has a negative sign before the radical and was consequently discarded as an extraneous root because it will not satisfy equations (23) in the limit as β_s tends to zero.

From this point on, $\bar{B}^2$ can be regarded as a known quantity, since the right-hand side of equation (E3) is expressed completely in terms of the given variables. With $\bar{B}^2$ now completely determined, $\cos 2\bar{\Delta}$ can be found from equation (E1). Similarly, $\sin 2\bar{\Delta}$ is given in terms of $\bar{A}$, Ω, ϵ, and β_s by equation (E2).

From an operational standpoint, it is now a straightforward problem to compute $\bar{B}$, $\bar{\Delta}$, G_n, and $\bar{\Phi}$. With $\bar{A}$, Ω, ϵ, β_s, and β_c given, $\bar{B}^2$ is found from equation (E3). Then $\sin 2\bar{\Delta}$ and $\cos 2\bar{\Delta}$ are computed by using equations (E1) and (E2). These results are all substituted into equations (23a) and (23b) which are repeated here for convenience

$$G_n \cos \bar{\Phi} = \left(1 - \Omega^2\right)\bar{A} - \frac{\epsilon\Omega^2\bar{A}}{4}\left(\bar{A}^2 - \bar{B}^2\cos 2\bar{\Delta}\right)$$

$$G_n \sin \bar{\Phi} = -2\beta_c\Omega\bar{A} - \frac{\epsilon\Omega^2\bar{A}}{4}\bar{B}^2\sin 2\bar{\Delta}$$

and which relate the unknown quantities on the left to the known variables on the right. The nondimensional force G_n and the phase $\bar{\Phi}$ can then be found from trigonometric identities; that is,

$$G_n = \left(G_n^2\cos^2\bar{\Phi} + G_n^2\sin^2\bar{\Phi}\right)^{1/2} \tag{E4}$$

and

$$\bar{\Phi} = \tan^{-1}\left(\frac{G_n \sin \bar{\Phi}}{G_n \cos \bar{\Phi}}\right) \tag{E5}$$

where $G_n \cos \bar{\Phi}$ and $G_n \sin \bar{\Phi}$ are computed from equations (23a) and (23b).

Similarly, $\bar{\Delta}$ can be determined as

$$\bar{\Delta} = \frac{1}{2}\tan^{-1}\left(\frac{\sin 2\bar{\Delta}}{\cos 2\bar{\Delta}}\right) \tag{E6}$$

since $\sin 2\bar{\Delta}$ and $\cos 2\bar{\Delta}$ are known from equations (E1) and (E2). Finally, $\bar{B}$ and $\bar{\psi}$ are easily obtained, since

$$\bar{B} = \sqrt{\bar{B}^2} \tag{E7}$$

and

$$\bar{\psi} = \bar{\Delta} + \bar{\Phi} \tag{E8}$$

where $\bar{B}^2$, $\bar{\Delta}$, and $\bar{\Phi}$ are all known from preceding calculations.

This approach was used to obtain curves of the variations of $\bar{A}$ with G_n, $\bar{B}$ with G_n, and so forth for particular values of Ω. By cross plotting the results, the response curves of figure 5 were obtained. The damping coefficients, β_s and β_c, and the nonlinearity parameter ϵ were held fixed during the calculations. The actual numerical work was done on an IBM 7090 electronic data processing system by using a simple FORTRAN program.

By using a large value of β_s in the calculations, the companion mode was suppressed and only the driven mode responded. This technique allowed the same program to be used to compute both the one- and two-mode response curves. Plots of $\bar{\Phi}$ against Ω and $\bar{\psi}$ against Ω were also made, but they are not presented here since the phase of the response is of relatively minor interest. For the coupled-mode case, however, it is interesting to note that $\bar{\Delta}$ was usually close to zero. Both $\bar{\Phi}$ and $\bar{\psi}$ ranged from $-\pi$ to $-\pi/2$ as the frequency ratio varied from $\Omega \gg 1$ down to $\Omega \approx 1$. Similar results were obtained for the single-mode response.

APPENDIX F

STABILITY OF THE COUPLED-MODE RESPONSE

As in the investigation of the stability of the single-mode response (appendix D), the stability of the coupled-mode response (eqs. (24)) may be examined by disturbing ζ_c and ζ_s directly:

$$\zeta_c(\tau) = \bar{A} \cos\left(\Omega\tau + \bar{\Phi}\right) + \xi_c(\tau)$$

$$\zeta_s(\tau) = \bar{B} \sin\left(\Omega\tau + \bar{\psi}\right) + \xi_s(\tau)$$

In the present case, however, this procedure results in two very complicated coupled differential equations involving ξ_c and ξ_s, with each term in the equations having a periodic coefficient. A simpler analysis (which is adequate for purposes of this report) can be made by the method of averaging.

Use of the Method of Averaging

To apply the method of averaging to the stability problem, let

$$\left.\begin{aligned} \bar{A} &= \bar{A}_o + a(\tau) \\ \bar{B} &= \bar{B}_o + b(\tau) \\ \bar{\Phi} &= \bar{\Phi}_o + \varphi(\tau) \\ \bar{\psi} &= \bar{\psi}_o + \gamma(\tau) \end{aligned}\right\} \tag{F1}$$

where the steady-state solution has been redesignated by

$$\left.\begin{aligned} \zeta_c(\tau) &= \bar{A}_o \cos\left(\Omega\tau + \bar{\Phi}_o\right) \\ \zeta_s(\tau) &= \bar{B}_o \sin\left(\Omega\tau + \bar{\psi}_o\right) \end{aligned}\right\} \tag{F2}$$

The variables $a(\tau)$, $b(\tau)$, $\varphi(\tau)$, and $\gamma(\tau)$ represent small perturbations in the amplitudes and phases of the steady-state response. The solution (eqs. (24) or (F2)) is said to be stable if a, b, φ, and γ do not increase with time.

Substituting the preceding expressions for $\bar{A}$, $\bar{B}$, $\bar{\Phi}$, and $\bar{\psi}$ (eqs. F1)) into equations (21) and retaining only first-order terms in the perturbations gives coupled equations of the form

$$c_{1j}a + c_{2j}\frac{da}{d\tau} + c_{3j}b + c_{4j}\frac{db}{d\tau} + c_{5j}\varphi + c_{6j}\frac{d\varphi}{d\tau} + c_{7j}\gamma + c_{8j}\frac{d\gamma}{d\tau} = 0 \tag{F3}$$

The index j ranges from 1 to 4 and corresponds to each of the equations (21a) to (21d). The coefficients c_{ij} are independent of τ and depend upon such quantities as the original amplitudes, phases, and damping. For any set of steady-state values $\left(\overline{A}_o, \ \overline{B}_o, \ \Omega, \ \epsilon, \text{ etc.}\right)$ the values of c_{ij} are constant, and equation (F3) then represents a system of linear equations with constant coefficients.

Such equations are readily solved by standard techniques. For example, when the substitutions

$$a(\tau) = a_1 e^{\lambda\tau}$$

$$b(\tau) = b_1 e^{\lambda\tau}$$

$$\varphi(\tau) = \varphi_1 e^{\lambda\tau}$$

$$\gamma(\tau) = \gamma_1 e^{\lambda\tau}$$

are made in equation (F3), an eigenvalue problem for λ results:

$$\left|L - \lambda M\right| = 0 \tag{F4}$$

where L and M are real, nonsymmetric four-by-four matrices involving the constants c_{ij}; a_1, b_1, φ_1, and γ_1 are also constants. When equation (F4) is multiplied out, it gives a polynomial which yields complex roots λ_i. If any root has a positive real part, the perturbations increase with time and the steady-state solution $\left(\overline{A}_o, \ \overline{B}_o, \ \Omega, \text{ etc.}\right)$ is unstable at that point. Conversely, the vibrations are stable if all the roots λ_i have negative real parts.

The Stability Boundaries and Their Interpretation

For the case of no damping $\left(\beta_c = 0, \ \beta_s = 0\right)$, equation (F4) can readily be expanded to give

$$\Lambda^4 + 2\alpha^2\left(\alpha^2 + \beta^2\right)\Lambda^2 + \alpha^2\beta^2\left(\alpha^2 - \beta^2\right) = 0 \tag{F5}$$

where the substitutions

$$\Lambda = 2\Omega\lambda$$

$$\alpha^2 = \frac{\epsilon\Omega^2\overline{A}_o^{\,2}}{2}$$

$$\beta^2 = \frac{\epsilon\Omega^2\overline{B}_o^{\,2}}{2}$$

have been used for simplification. The roots of equation (F5) will have negative real parts if the inequality

$$1 - \frac{2.38\epsilon\bar{A}_o^2}{8} + O(\epsilon^2) < \Omega \tag{F6}$$

is satisfied.

On the other hand, in the absence of damping, equation (23c) shows that real nonzero values of $\bar{B}$ will exist only if Ω meets the condition

$$\Omega \leqq 1 + \frac{\epsilon\bar{A}^2}{8} + O(\epsilon^2) \tag{F7}$$

(Note that this condition agrees with that in the one-mode stability analysis.) (See appendix D.) The preceding inequalities combine to show that the approximate solution (eqs. (24)) is real valued and stable (in the absence of damping) within the region

$$1 - \frac{2.38\epsilon\bar{A}^2}{8} + O(\epsilon^2) < \Omega < 1 + \frac{\epsilon\bar{A}^2}{8} + O(\epsilon^2) \tag{F8}$$

The results of the coupled-mode stability analysis are presented in figure 7. Real values of $\bar{B}$ do not exist to the right of the curve $\Omega = 1 + \frac{\epsilon\bar{A}^2}{8}$, and the two-mode solution is unstable to the left of the curve $\Omega = 1 - \frac{2.38\epsilon\bar{A}^2}{8}$. Damping alters these stability boundaries, primarily near $\Omega = 1$ and for small values of $\bar{A}$. The effect of a small amount of damping is indicated qualitatively in figure 7 by the dashed lines.

APPENDIX G

TECHNICAL DETAILS OF EXPERIMENTS

For reasons of conciseness and readability, it was necessary to omit from the body of the report many of the technical details pertaining to the experiments. The purpose of this appendix is to explain some of these experimental intricacies which include the measurement of the forcing function and the analysis of the response by means of Lissajous figures.

Equipment for Measuring Deflections

Radial motions of the ring were measured by two inductance pickups. These deflection sensors were mounted on a fixture with a large bearing which allowed them to move circumferentially around the ring. (See figs. 12 and 13.) The signal from each pickup was fed through a carrier

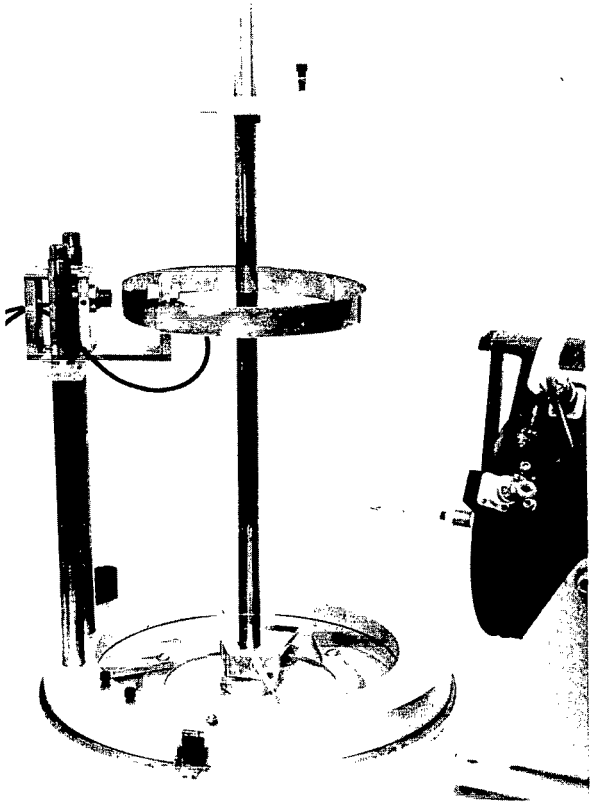

Figure 12.- Overall view of experimental setup. L-65-7901

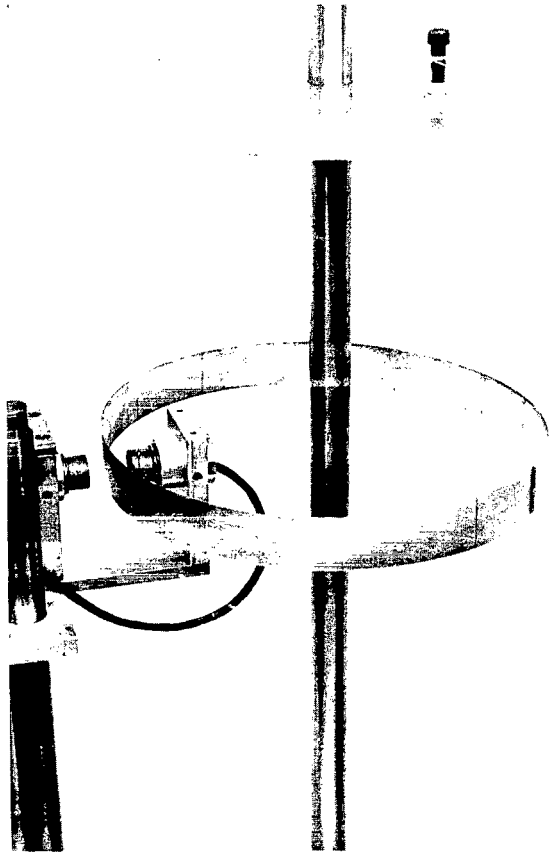

Figure 13.- Closeup of ring. L-65-7902

amplifier and into one side of a differential amplifier, the output of which was in turn sent through a band-pass filter to a cathode-ray oscilloscope (CRO). (A block diagram of the arrangement is shown in fig. 8.) The system was connected so that the pickups operated in a push-pull fashion; this arrangement resulted in an antisymmetric operating characteristic, shown in figure 14.

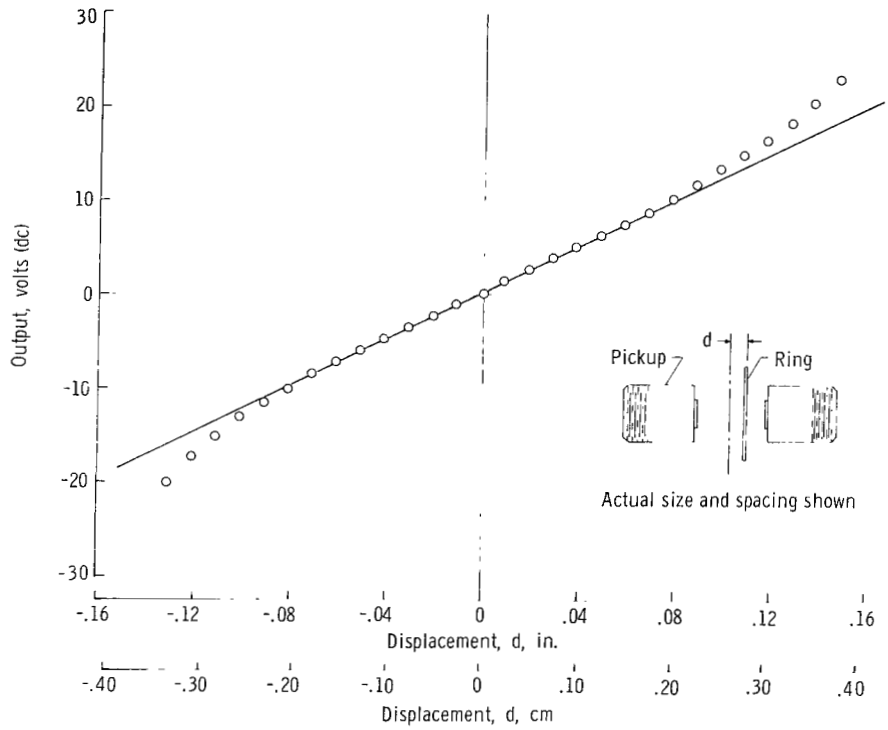

Figure 14.- Calibration curve for pickup system.

Application and Measurement of Forcing Function

Vibrations of the ring were excited by means of an electrodynamic shaker. The shaker was connected to the ring by a fine tungsten drive wire (0.001-inch (0.003-cm) diameter), as shown in figures 12 and 13. The wire served as a very soft coupling spring between the shaker and the ring. Soft coupling was imperative, since the spring acted as a constraint and raised the effective natural frequency of the ring.

The shaker amplitude and frequency were controlled by a standard oscillator-amplifier arrangement. By recording the displacement of the shaker and knowing the spring constant of the wire, it was possible to compute the force acting on the ring. That is, for a shaker displacement of $\delta_o \cos \omega t$, the amplitude of the force exerted on the ring was

$$P = \frac{1}{2} k\delta_o \tag{G1}$$

where k is the spring constant of the drive wire, δ_o is the amplitude of

the shaker displacement, and the factor 1/2 arises from the geometry of the drive-wire arrangement. Strictly speaking, equation (G1) applies only for static displacements of the coupling spring. However, when the fundamental resonant frequency of the coupling spring is much higher than the frequency supplied by the shaker, the equation $P = \frac{1}{2} k\delta_o$ becomes a very good approximation. In this case, the inertia of the coupling spring can be neglected, and the spring displacements are quasi-static.

Although other types of coupling springs were tried, it was found that the tungsten drive wire was the only one which could satisfy the conflicting requirements of soft coupling (i.e., a low value of k) and high resonant frequency. The wire used in the experiments had a fundamental frequency of 300 cps (300 Hz) and a spring constant of only 0.035 lb/in. (6.12 N/m).

Because of its low stiffness, the drive wire had only a slight influence on the natural frequencies of the ring. However, its attachment to the ring was such that the frequencies of the $\cos \frac{ny}{R}$ modes were raised slightly, whereas those of the $\sin \frac{ny}{R}$ modes were unaffected. This disparity created an overlapping of two instability regions (fig. 15) and led to anomalous results. To counteract this effect, it was necessary to add a small concentrated mass to an antinode of $\cos \frac{ny}{R}$, which lowered its natural frequency and separated the unstable regions.

Adding the small mass had another beneficial effect, as it greatly reduced the tendency of the nodes of $\cos \frac{ny}{R}$ to "drift" circumferentially. Such shifting of the nodes can be explained by considering small imperfections in the ring, as noted by Tobias (ref. 27). The added mass was a short piece of solder which was glued to the ring directly alongside the drive wire. This arrangement fixed the "preferential modes" of the ring. (See ref. 27.)

The location of the mass and the drive wire may be thought of as the origin of the circumferential coordinate y. In this case, the force exerted on the ring acts at y = 0. As a consequence, the $\cos \frac{ny}{R}$ modes were driven by the forcing

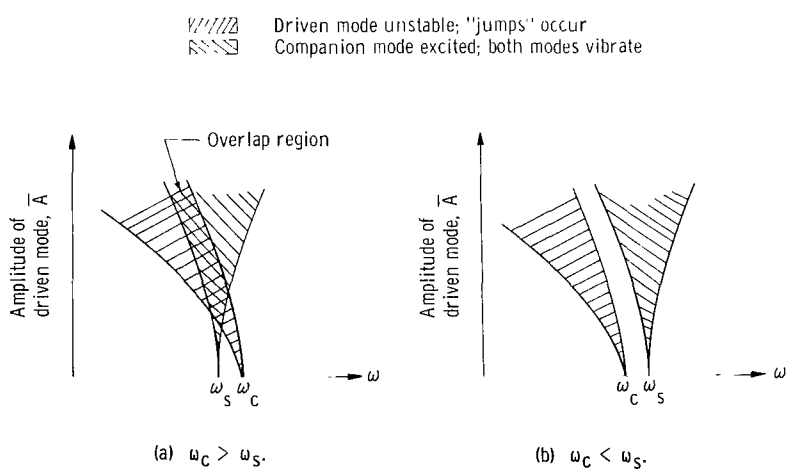

Figure 15.- Shift of instability regions due to changes in natural frequency. ω_c = Linear frequency of $\cos \frac{ny}{R}$; driven mode. ω_s = Linear frequency of $\sin \frac{ny}{R}$; companion mode.

function, but the $\sin \frac{ny}{R}$ modes were not; that is, there was no generalized force on the $\sin \frac{ny}{R}$ modes. Note that the analysis was conducted for a similar case.

Actually, the loading used in the analysis (eq. (13)) was

$$q(y,t) = \frac{F_n}{\pi R} \cos \frac{ny}{R} \cos \omega t$$

whereas the experimental loading was concentrated at $y = 0$ and can be represented as

$$q(y,t) = \delta(y) F \cos \omega t \tag{G2}$$

In equation (G2), $\delta(y)$ is the Dirac delta function and F is the load per unit length that the drive wire exerts on the ring. For the experimental arrangement described herein, F can be calculated from

$$F = \frac{P}{b} \tag{G3}$$

where b is the length of the ring and P is given by equation (G1).

This type of loading (eq. (G2)) is analyzed in reference 15. The results are very similar to those of the present analysis, provided that the driving frequency ω is in the vicinity of the natural frequency of the $\cos \frac{ny}{R}$ mode. In this case, the response of the ring can be approximated by using F in place of F_n in equation (13) and other related equations. For example, the corresponding nondimensional force G_n becomes

$$G_n = \frac{F}{\pi R \rho h^2 \omega_M^2} = \frac{P}{(\pi R \rho h b) h \omega_M^2} \tag{G4}$$

where equation (G3) has been used.

A more detailed explanation of the experimental apparatus is given in reference 15; as indicated therein, refined experimental techniques were used to minimize the nonlinearities introduced by the measuring system and by the suspension, shaker, and drive arrangement.

Analysis of Response

Detection of a single mode.- As noted previously, the pickup system sensed radial motions of the ring and converted them into electrical signals which were displayed on an oscilloscope. These signals were interpreted with the aid of Lissajous figures, as follows:

APPENDIX G

The voltage proportional to the radial displacement of the ring was fed into the vertical axis of the oscilloscope, while the horizontal axis was driven by the oscillator which controlled the shaker. This arrangement resulted in a Lissajous figure which indicated both the amplitude and the phase of the vibration that was being sensed by the pickup. By slowly moving the pickup around the circumference of the ring and noting the successive Lissajous figures, it was possible to analyze the motion of the ring. For example, when the response consisted of primarily the $\cos \frac{ny}{R}$ mode vibrating near its resonant frequency, successive Lissajous patterns such as those shown in figure 16 were observed. The open vertical ellipses indicated that the major response was $\pm 90^{\circ}$ out of phase with the forcing function; measurements showed that the amplitude of the response varied as $\cos \frac{ny}{R}$ around the circumference. At the zeros of $\cos \frac{ny}{R}$, the Lissajous figures were small horizontal figure eights which indicated vibrations at twice the driving frequency. This pattern was in agreement with the analytical results, which predicted the occurrence of this type of "double-frequency contraction."

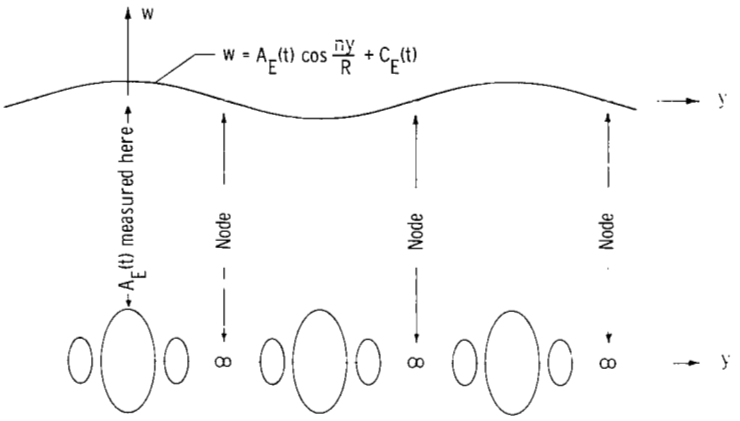

Figure 16.- Circumferential variation of Lissajous figures. Single-mode response (resonance).

These observations were in general agreement with the assumed vibration mode; namely,

$$w(y,t) = A_n(t) \cos \frac{ny}{R} - \frac{n^2}{4R} A_n^2(t) \qquad (G5)$$

where $A_n(t) \sim \cos \omega t$. Subsequent measurements around the circumference of the ring supported this conclusion.

Circumferential variation of response.- The voltage V from the pickup system can be represented as a Fourier series in time

$$V(y,t) = V_1(y) \cos \omega t + V_2(y) \cos 2\omega t + V_3(y) \cos 3\omega t + \ldots \qquad (G6)$$

with coefficients that vary around the circumference of the ring. The coefficients, $V_1(y)$, $V_2(y)$, . . ., contain the spatial variation of the deflection shape, combined with the harmonics introduced by the pickup system. By passing the signal through a harmonic analyzer and using a narrow 2-cps (2-Hz) band-pass

filter, the circumferential variation of the first, second, and third harmonics was determined. This determination was accomplished by exciting the $n = 4$ mode and recording the appropriate voltages at several positions along a half wavelength. The results are given in nondimensional form in figure 17. The relative amplitudes of the harmonics were in the ratio

$$V_{1,max} : V_{2,node} : V_{3,max} \quad \text{as } 1 : 0.04 : 0.018$$

As shown in figure 17, $V_1(y)$ was almost a perfect sine wave. Similar results were obtained for other half waves of the $n = 4$ mode and led to the conclusion that $V_1(y)$ was very closely represented by $V_{1,max} \cos \frac{ny}{R}$. It is believed that this voltage variation was due entirely to the motion of the ring, that is,

$$w(y,t) \sim A \cos \omega t \cos \frac{ny}{R}$$

would give rise to the observed results.

The variation of the other harmonics was influenced by the nonlinearities of the pickup system which made it impossible to determine how much of the $\cos 2\omega t$ term was caused by actual motion of the ring. As indicated in figure 17, however, $V_2(y)$ did contain a major component that was constant in space, as is suggested by the theory.

The third harmonic in the signal resulted primarily from the nonlinearity of the pickup system. The data indicated that $V_3(y)$ varied as $V_{3,max} \sin^3 \pi r$, where r is the fraction of the half wavelength. Such a result can be explained by considering the antisymmetric operating characteristic of the pickup system and noting that the major input to the system (i.e., the deflection of the ring) varied as $\sin \pi r$ along a half wave. The latter result was confirmed by subsequent mode-shape measurements which showed that the primary deflection of the ring was independent of the vibration amplitude. (See fig. 9 and the related discussion in the body of this report.)

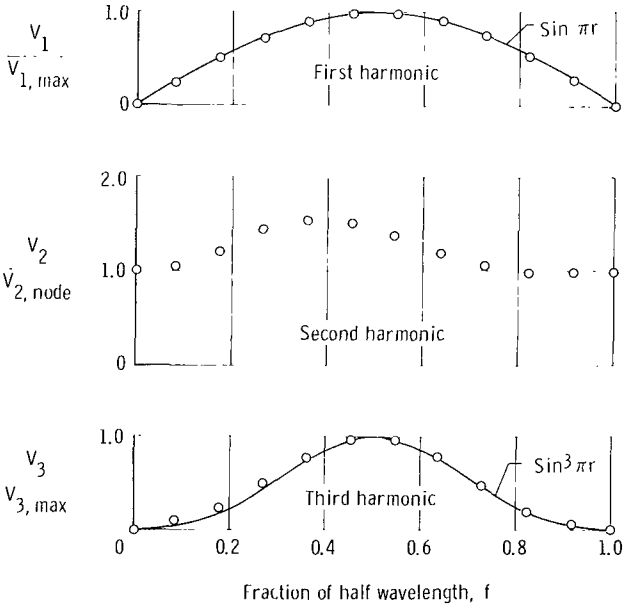

Figure 17.- Spatial variation of response voltage. Amplitude of vibration: $A_{max} = 16.1h$.

Additional results (ref. 15) include a plot of the root-mean-square response around the circumference of the ring and measurement of the amplitude of the "double-frequency contraction" at the nodes

of $\cos \frac{ny}{R}$. The conclusion from all these measurements was that the experimental deflection could be expressed as

$$w(y,t) = A_E(t)\cos \frac{ny}{R} + C_E(t) \tag{G7}$$

when Lissajous figures of the type shown in figure 16 were observed. Amplitudes $A_E(t)$ and $C_E(t)$ are the experimental time-varying amplitudes of $\cos \frac{ny}{R}$ and the uniform contraction, respectively. The amplitude $A_E(t)$ was measured at the antinodes of $\cos \frac{ny}{R}$, whereas the contraction $C_E(t)$ was measured at the nodes.

Detection of two coupled modes.- Early in the experimental program, it was noticed that in some cases small changes in the driving frequency ω caused significant modifications of the Lissajous patterns. This behavior was traced to the appearance of the companion mode $\sin \frac{ny}{R}$, which participated in the motion along with the $\cos \frac{ny}{R}$ mode.

When coupled vibrations of this type occurred, successive Lissajous patterns such as those shown in figure 18 were obtained. The open vertical ellipses were observed at the antinodes of $\cos \frac{ny}{R}$ and indicated that the response there was $\pm 90^\circ$ out of phase with the input force. At the nodes of $\cos \frac{ny}{R}$, the Lissajous figures were straight lines, which is characteristic of a response directly in (or out of) phase with the input. The straight lines resulted from the $\sin \frac{ny}{R}$ mode, which has its maximum amplitude at the nodes of $\cos \frac{ny}{R}$. After trying various combinations of sines and cosines, it was found that the observed Lissajous figures correspond to a deflection of the form

$$w(y,t) = A \cos(\omega t + \Phi_A)\cos \frac{ny}{R} + B \sin(\omega t + \Phi_B)\sin \frac{ny}{R} \tag{G8}$$

which demonstrates the existence of the companion mode.

When the amplitudes (A and B) and the phases (Φ_A and Φ_B) of the motion are exactly equal, a pure traveling wave results. That is, equation (G8) may then be written in the form

$$w(y,t) = A \cos\left[\frac{ny}{R} - (\omega t + \Phi_A)\right] \tag{G9}$$

Observations with the aid of a stroboscope disclosed the presence of traveling waves when Lissajous patterns such as those in figure 18 were noted. These observations gave further indication that the coupled vibration involved the $\cos \frac{ny}{R}$ mode and its companion mode $\sin \frac{ny}{R}$.

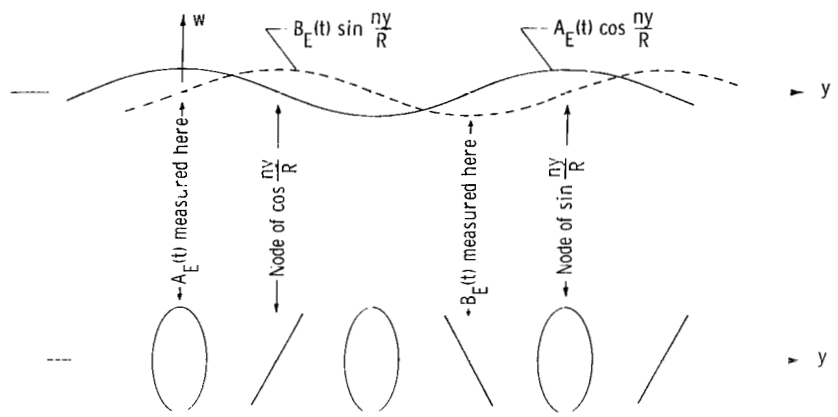

Figure 18.- Circumferential variation of Lissajous figures. Coupled-mode response (resonance).

It was also noted that the appearance of the companion mode resulted in a reduction of the second harmonic content of the response. This result is in agreement with the analysis, as may be seen by examining the contraction term (eq. (9))

$$A_o(t) = - \frac{n^2}{4R}\left[A_n^2(t) + B_n^2(t)\right]$$

Since $A_n(t)$ and $B_n(t)$ are out of phase by 90° (i.e., $A_n \sim \cos \omega t$, $B_n \sim \sin \omega t$), the second harmonic component of $A_n^2(t)$ tends to cancel that of $B_n^2(t)$ when the two terms are added.

As a result of these and other observations, it was concluded that the experimental deflection could be expressed as

$$w(y,t) = A_E(t)\cos \frac{ny}{R} + B_E(t)\sin \frac{ny}{R} + C_E(t) \qquad (G10)$$

when Lissajous figures of the type shown in figure 18 were observed. The coefficients $A_E(t)$, $B_E(t)$, and $C_E(t)$ are the experimental time-varying amplitudes of $\cos \frac{ny}{R}$, $\sin \frac{ny}{R}$, and the uniform contraction, respectively.

Once the various responses of the ring had been identified, it was possible to obtain response curves of the variations of $A_E(t)$ and $B_E(t)$ with ω and to compare them with the analytical results. These tests are described in the body of the report.

APPENDIX G

Other Results of Interest

In addition to the preceding results, several other experimental observations were made. Part of this work was an experimental response survey, the results of which are given in table I. As indicated therein, several ultraharmonic responses were noted, including some which involved coupling between two modes with different mode numbers. Results of this type are predicted by the infinite mode analysis of reference 15. Additional experiments reported in reference 15 include the steady-state response of the $n = 3$ mode and some transient responses of the $n = 4$ mode. The latter responses demonstrate the growth of the companion mode with time when the driven mode exceeds the critical amplitude. Damping traces were also obtained for the $n = 3$ and $n = 4$ modes. For these and other details, see reference 15.

APPENDIX H

ANALOG-COMPUTER STUDIES

The approximate solutions obtained by the method of averaging indicate a gap in the coupled-mode-response curves. In order to find out what happens to the response in the gap region, an analog computer was used to simulate equations (12) which are repeated here for convenience.

$$\frac{d^2\zeta_c}{d\tau^2} + 2\beta_c \frac{d\zeta_c}{d\tau} + \zeta_c + \frac{\epsilon}{2}\zeta_c\left[\zeta_c \frac{d^2\zeta_c}{d\tau^2} + \left(\frac{d\zeta_c}{d\tau}\right)^2 + \zeta_s \frac{d^2\zeta_s}{d\tau^2} + \left(\frac{d\zeta_s}{d\tau}\right)^2\right] = G_n \cos \Omega\tau$$

$$\frac{d^2\zeta_s}{d\tau^2} + 2\beta_s \frac{d\zeta_s}{d\tau} + \zeta_s + \frac{\epsilon}{2}\zeta_s\left[\zeta_s \frac{d^2\zeta_s}{d\tau^2} + \left(\frac{d\zeta_s}{d\tau}\right)^2 + \zeta_c \frac{d^2\zeta_c}{d\tau^2} + \left(\frac{d\zeta_c}{d\tau}\right)^2\right] = 0$$

Analog-computer solutions were obtained for both the coupled-mode and single-mode responses. The procedure used and the results obtained are briefly discussed in the following paragraphs.

In setting up the analog procedure, the parameters β_c, β_s, ϵ, and G_n were held constant, and responses were obtained at various values of Ω. The procedure used was to set all the initial conditions equal to zero $\left(\text{i.e., } \zeta_c(0) = 0, \frac{d\zeta_c}{d\tau}(0) = 0, \text{ etc.}\right)$ and then turn on the forcing function at a particular frequency Ω. The driven mode would respond to the excitation, and usually it would reach a steady state, whether or not the companion mode also responded. Once steady-state conditions were attained, the stability of the response was examined by intentionally "bumping" or disturbing ζ_c and ζ_s electrically. When the companion mode did not respond, disturbances to ζ_s were found to damp out, as would be expected. Responses were obtained for two distinct cases which differ in the amount of damping in the companion mode.

Case 1: coupled-mode response.- In the case of the coupled-mode response, the parameters used were

$$\beta_c = \beta_s = 0.002 \quad \text{(equal damping in both modes)}$$

$$\epsilon = 4.2 \times 10^{-4} \quad \text{(nonlinearity)}$$

$$G_n = 0.1 \quad \text{(force)}$$

These values are the same as those used to calculate the coupled-mode response by the method of averaging. As shown in figure 5, the analog results agreed

very well with the analytical solutions. In the gap region, the analog traces indicated nonsteady vibrations with beats. It was impossible to obtain steady-state responses within the gap, even though the problem was run for several hundred cycles.

Case 2: single-mode response.- In the case of the single-mode response, the companion mode was heavily damped to prevent its vibration. The parameters used were the same as the preceding case except for β_s which was $\beta_s = 0.05$ (companion mode damped heavily relative to the driven mode). The analog results verified the analytical solution for this case, as shown in figure 2.

REFERENCES

1. Reissner, Eric: Non-Linear Effects in the Vibrations of Cylindrical Shells. Rept. No. AM 5-6, Guided Missile Res. Div., Ramo-Wooldridge Corp., Sept. 30, 1955.

2. Chu, Hu-Nan: Influence of Large Amplitudes on Flexural Vibrations of a Thin Circular Cylindrical Shell. J. Aerospace Sci., vol. 28, no. 8, Aug. 1961, pp. 602-609.

3. Cummings, Benjamin E.: Some Nonlinear Vibration and Response Problems of Cylindrical Panels and Shells. SM 62-32 (AFOSR 3123), Graduate Aeron. Labs., C.I.T., June 1962.

4. Evensen, David A.: Some Observations on the Nonlinear Vibration of Thin Cylindrical Shells. AIAA J. (Tech. Notes and Comments), vol. 1, no. 12, Dec. 1963, pp. 2857-2858.

5. Hoppe, R.: Vibrationen eines Ringes in seiner Ebene. J. Reine Angewante Math., Bd. LXXIII, Heft 2, 1871, pp. 158-170.

6. Rayleigh (Lord): The Theory of Sound. First Am. ed., vols. I and II, Dover Publ., 1945.

7. Philipson, L. L.: On the Role of Extension in the Flexural Vibrations of Rings. J. Appl. Mech., vol. 23, no. 3, Sept. 1956, pp. 364-366.

8. Buckens, F.: Influence of the Relative Radial Thickness of a Ring on its Natural Frequencies. J. Acoust. Soc. Am., vol. 22, no. 4, July 1950, pp. 437-443.

9. Federhofer, Von K.: Biegungsschwingungen eines Kreisringes bei konstantem Aussen-oder Innendrucke. Ingr.-Arch., Bd. IV, Heft 2, Apr. 1933, pp. 110-120.

10. Federhofer, Von Karl: Nicht-lineare Biegungsschwingungen des Kreisringes. Ingr.-Arch., Bd. XXVIII, 1959, pp. 53-58.

11. Shkenyev, Yu. S.: Nelineyniye Kolebaniya Krugovogo Kol'tsa. Inzh. Sb., vol. XXVIII, 1960, pp. 82-86.

12. Goodier, J. N.; and McIvor, I. K.: Dynamic Stability and Non-Linear Oscillations of Cylindrical Shells (Plane Strain) Subjected to Impulsive Pressure. Tech. Rept. No. 132 (Contract Nonr 255(29)), Div. Eng. Mech., Stanford Univ., June 1962.

13. Kaiser, Elmer R.: Acoustical Vibrations of Rings. J. Acoust. Soc. Am., vol. 25, no. 4, July 1953, pp. 617-623.

14. Lang, T. E.: Vibration of Thin Circular Rings. Pt. 1. Solutions for Modal Characteristics and Forced Excitation. Tech. Rept. No. 32-261 (Contract No. NAS 7-100), Jet Propulsion Lab., C.I.T., July 1, 1962.

15. Evensen, David Authur: Non-Linear Flexural Vibrations of Thin Circular Rings. Ph. D. Thesis, California Inst. Technol., 1964.

16. Mechtly, E. A.: The International System of Units - Physical Constants and Conversion Factors. NASA SP-7012, 1964.

17. Oplinger, Donald W.: Frequency Response of a Nonlinear Stretched String. J. Acoust. Soc. Am., vol. 32, no. 12, Dec. 1960, pp. 1529-1538.

18. Woinowsky-Krieger, S.: The Effect of an Axial Force on the Vibration of Hinged Bars. J. Appl. Mech., vol. 17, no. 1, Mar. 1950, pp. 35-36.

19. Chu, Hu-Nan; and Herrmann, George: Influence of Large Amplitudes on Free Flexural Vibrations of Rectangular Elastic Plates. J. Appl. Mech., vol. 23, no. 4, Dec. 1956, pp. 532-540.

20. Singer, Josef: On the Equivalence of the Galerkin and Rayleigh-Ritz Methods. J. Roy. Aeron. Soc., vol. 66, no. 621, Sept. 1962, p. 592.

21. McLachlan, N. W.: Ordinary Non-Linear Differential Equations in Engineering and Physical Sciences. Second ed., The Clarendon Press (Oxford), 1956.

22. Hutton, R. E.: An Investigation of Resonant, Nonlinear, Nonplanar Free Surface Oscillations of a Fluid. NASA TN D-1870, 1963.

23. Miles, John W.: Stability of Forced Oscillations of a Spherical Pendulum. Quart. Appl. Math., vol. XX, no. 1, Apr. 1962, pp. 21-32.

24. Herrmann, G.; and Armenakas, A. E.: Dynamic Behavior of Cylindrical Shells Under Initial Stress. AFOSR TN-60-425, U.S. Air Force, Apr. 1960. (Available from ASTIA as AD No. 237 901.)

25. Morley, L. S. D.: An Improvement on Donnell's Approximation for Thin-Walled Circular Cylinders. Quart. J. Mech. Appl. Math., vol. XII, pt. 1, 1959, pp. 89-99.

26. Stoker, J. J.: Nonlinear Vibrations in Mechanical and Electrical Systems. Interscience Publ. Inc., c.1950.

27. Tobias, S. A.: Free Undamped Non-Linear Vibrations of Imperfect Circular Disks. Proc. Inst. of Mech. Engrs., vol. 171, no. 22, 1957, pp. 691-715.

TABLE I.- EXPERIMENTAL RESPONSE SURVEY

Mode vibrating	Driving frequency, cps or Hz	Type of response
n = 2	7.1	Resonance at driving frequency
n = 3	17.5	
n = 4	33.0	
n = 5	53.2	
n = 6	78.0	
n = 7	107.4	
n = 8	139.2	
n = 9	179.6	
n = 10	222.8	
n = 3	8.8	Ultraharmonic; order 1/2
n = 4	11.1	Ultraharmonic; order 1/3
n = 7	213.0	Subharmonic; order 2
n = 8	69.8	Ultraharmonic; order 1/2
n = 8	47.6	Ultraharmonic; order 1/3
n = 9	92.3	Ultraharmonic; order 1/2
n = 3, n = 5	26.7	n = 3 at 26.7 cps (Hz); n = 5 at 53.4 cps (Hz)
n = 4, n = 6	39.0	n = 4 at 39.0 cps (Hz); n = 6 at 78.0 cps (Hz)
n = 4, n = 7	35.8	n = 4 at 35.8 cps (Hz); n = 7 at 107.4 cps (Hz)
n = 4, n = 8	35.3	n = 4 at 35.3 cps (Hz); n = 8 at 141.2 cps (Hz)
n = 5, n = 9	60.5	n = 5 at 60.5 cps (Hz); n = 9 at 181.5 cps (Hz)

NASA-Langley, 1965 L-4216

"The aeronautical and space activities of the United States shall be conducted so as to contribute . . . to the expansion of human knowledge of phenomena in the atmosphere and space. The Administration shall provide for the widest practicable and appropriate dissemination of information concerning its activities and the results thereof."

—NATIONAL AERONAUTICS AND SPACE ACT OF 1958

NASA SCIENTIFIC AND TECHNICAL PUBLICATIONS

TECHNICAL REPORTS: Scientific and technical information considered important, complete, and a lasting contribution to existing knowledge.

TECHNICAL NOTES: Information less broad in scope but nevertheless of importance as a contribution to existing knowledge.

TECHNICAL MEMORANDUMS: Information receiving limited distribution because of preliminary data, security classification, or other reasons.

CONTRACTOR REPORTS: Technical information generated in connection with a NASA contract or grant and released under NASA auspices.

TECHNICAL TRANSLATIONS: Information published in a foreign language considered to merit NASA distribution in English.

TECHNICAL REPRINTS: Information derived from NASA activities and initially published in the form of journal articles.

SPECIAL PUBLICATIONS: Information derived from or of value to NASA activities but not necessarily reporting the results of individual NASA-programmed scientific efforts. Publications include conference proceedings, monographs, data compilations, handbooks, sourcebooks, and special bibliographies.

Details on the availability of these publications may be obtained from:

SCIENTIFIC AND TECHNICAL INFORMATION DIVISION

NATIONAL AERONAUTICS AND SPACE ADMINISTRATION

Washington, D.C. 20546